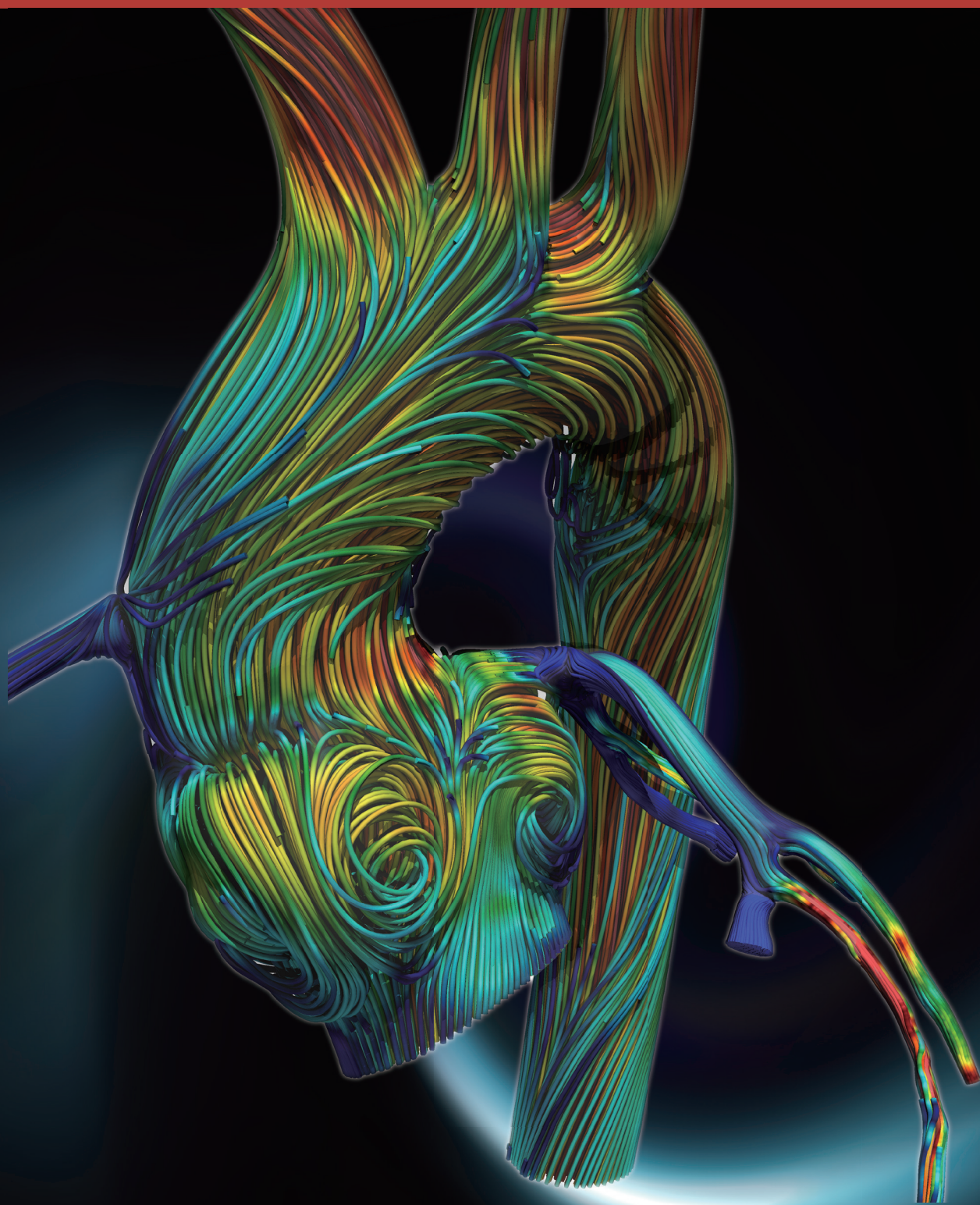


# An Encouragement of Blood Flow Analysis



**CARDIO FLOW DESIGN**

### Introduction.

Cardiovascular disease, represented by angina pectoris and myocardial infarction, has the highest mortality rate in the world.

It is well known that vortical and turbulent flow of blood occurs in the heart, and that this flow has a significant impact on the function of the heart. For this reason, research has been conducted worldwide to analyze blood flow in various cardiovascular diseases.

Mankind seems to have had a long-standing interest in the vortex flow of the heart. Leonardo da Vinci, a well-known Renaissance artist, left sketches depicting the vortices that arise within the heart.

In that era, of course, there was no way to measure the vortex flow inside the human body. However, da Vinci foresaw that the blood flow beating out of the heart would create a vortex around the valves and that the blood flow entering the heart would create a vortex around the tricuspid valve (Figure 1).

After da Vinci, blood flow in the heart was not systematically studied for some time, but after the development of the sphygmomanometer<sup>(1)</sup> in 1886, blood flow was measured by blood pressure.

Another 100 years later, in the 1990s, with the rise of computer technology, research using MRI and computer simulations finally made it possible for us to see the actual vortex flow of the heart.

Blood flow analysis, the theme of this booklet, is a field of research that combines the latest medical and IT technologies to visualize blood flow in moving images using state-of-the-art computer technology.

Specifically, our research includes such questions as "What kind of pathological blood flow occurs in cardiovascular disease and how does it aggravate the disease?" and "How does treatment improve blood flow and what kind of therapeutic effect can be expected?"

This booklet is intended for those who would like to start research on blood flow analysis, those who have already started but feel they do not understand it well, and those who would like to learn more about the mathematical formulas, etc. that form the basis of blood flow analysis.

We have tried to introduce the basics of blood flow, cutting-edge medical technology, and medical research in as simple a manner as possible. As a person involved in the development of blood flow analysis technology, We sincerely hope that your curiosity about medicine will open the door to tomorrow's medical research and, by extension, become the driving force to build the future of medicine.

November, 2022

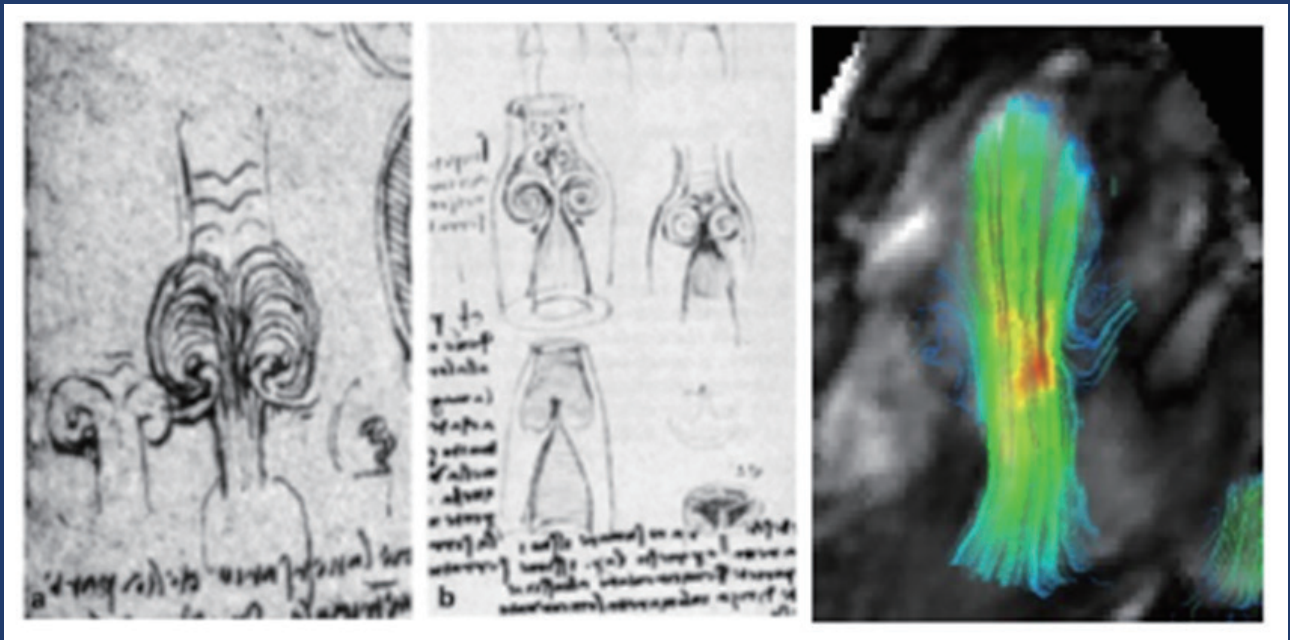


Figure 1 Leonardo da Vinci's sketch of blood flow in the sinus of Valsalva (left, middle). The sinus of Valsalva is the origin of the aorta connected from the left ventricle. On the right is actual blood flow captured by MRI.

# Table of contents

## Chapter 1: Blood Flow from Fluid Mechanics Perspective

### 1. Blood flow analysis

- Know the structure of the heart 6.
- Left ventricular blood flow 7.
- Left atrium blood flow 8.
- Aortic blood flow 9
- Blood flow in the right atrium and the right ventricle 10.
- Pulmonary artery blood flow 11.
- Characteristics of left and right heart systems 12.

### 2. Turbulence in the heart and blood vessels

- What is turbulence 13.
- Advantages of turbulence 13.
- What is Reynolds number? 14.
- Mechanism of vortex generation 15.

### 3. Relationship between blood pressure and blood flow

- What is the pressure range? 16.
  - (1) Energy loss caused by stenosis 17.
  - (2) Energy loss caused by impingement on vessel wall 18.
  - (3) Energy loss caused by vascular bending 18.
- Static and dynamic pressures of fluids 19.

## Chapter 2: Methods of Blood Flow Analysis

### 1. Three methods of blood flow analysis 21.

### 2. Computational fluid dynamics (CFD) - Simulation of fluid flow 22.

Strengths and Cautions / Application Examples / Data Necessary for Analysis

### 3. 4D Flow MRI -3D blood flow information in real time 23.

Strengths and Cautions / Data required for analysis

### 4. Ultrasonic measurement - Calculation of internal pressure range from measured data 24.

Strengths and Cautions / Application Examples / Data Necessary for Analysis

## Chapter 3: Examples of Blood Flow Analysis

### 1. Virtual surgical simulation (Valsalva aneurysm)

- Blood flow analysis reveals problems 26.
- Virtual surgical selected for artificial vascular reconstruction 26.

### 2. Blood flow analysis to determine treatment guidelines

Pulmonary valve regurgitation after TOF surgery

- Integrated data from 4D Flow MRI 27.



### **3. 4D Flow MRI blood flow analysis before and after treatment** (chronic aortic dissection)

- Actual measurement of blood flow in the false lumen changes over time after TEVAR 28.
- Primary entry closure significantly changes hemodynamics in the false lumen 29.

### **4. Surgical design of pulmonary angioplasty (congenital heart disease)**

- Virtual surgery to design the shape of the patch 30.
- Surgery is performed as simulated 31.

### **5. Revascularization by aortoplasty (congenital heart disease)**

- Determine aortic reconstructive procedures from ELI and WSS 31.
- Virtual surgery to confirm Pre- and post-operative changes 32.

### **6. Evaluation of intracardiac vortical flow after mitral valve surgery by VFM (mechanical and biological valves)**

- Performance varies depending on the aspect of the vortex flow 36.
- How does energy efficiency change with vortex orientation 37.

## **Chapter 4: Various Indicators for Blood Flow Analysis**

### **1. Flow velocity vector is a basic indicator**

- If you know the vectors, you know the whole process 35.
- How to visualize flow (1) [Streamlines] 35.
- How to visualize flow (2)[Pathlines] 36.

### **2. Energy loss (EL)**

- What causes the heart to lose pulsating energy? 37.
- Pressure information is essential for EL calculations 37.

### **3. Wall Shear Stress (WSS)**

- WSS can detect atherosclerosis and aneurysms 39.
- To obtain a reliable WSS value 40.
- OSI to quantify fluctuations in time variation 40.

### **4. Three indicators for vortex**

- Purposeful eddies and disorganized, harmful eddies exist 41.
- Vortex index (1) [Vorticity] 41.
- Vortex index (2) [Cycle] 42.
- Vortex index (3) [Helicity] 43.

[Appendix 1] Fluid Dynamics in Equations 44.

[Appendix 2] Paper Introduction 50.

[References] 55.

[Column] 56.

# Chapter 1: Blood Flow from Fluid Mechanics

## 1. Blood flow analysis

Know  
the structure  
of the heart

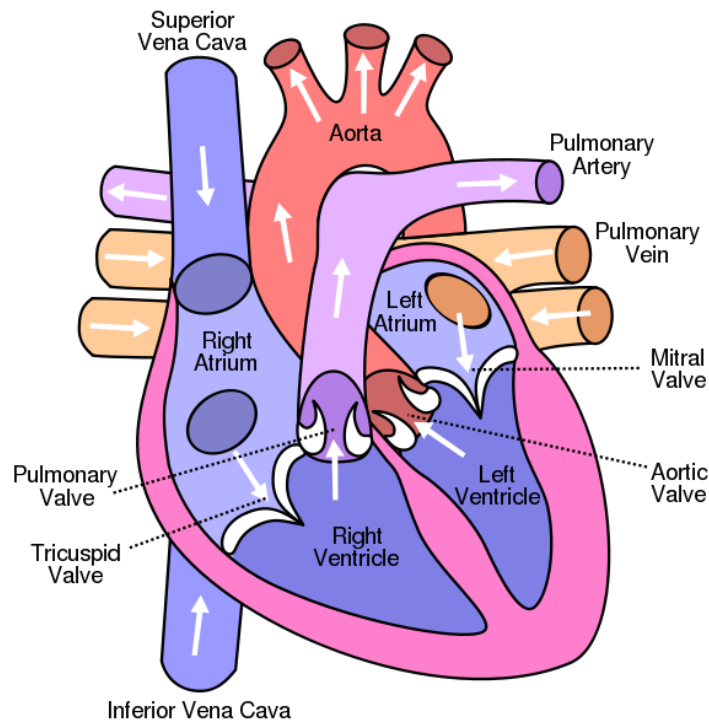
### Four chambers have back valves for blood.

The heart is divided into four chambers: the right atrium, right ventricle, left atrium, and left ventricle, each of which contracts and relaxes at a certain rhythm to pump blood throughout the body.

The left ventricle sends oxygen-rich red arterial blood throughout the body. The blood pulsed from the left ventricle travels through the "aorta," which curves more than 180 degrees, to the lower half of the body.

Venous blood that has finished transporting oxygen throughout the body flows through the superior vena cava into the right atrium. Blood is then sent from the right ventricle to the lungs, where it takes up a lot of oxygen, and then returns to the left atrium via two "pulmonary veins."

The left and right ventricles are equipped with anti-reflux valves to prevent blood from flowing backward. The left ventricle has the mitral valve at its entrance and an aortic valve at its exit. The right ventricle has the tricuspid valve at its entrance and a pulmonary valve at its exit.



The four chambers of the heart and the anti-reflux valve  
(The right side of the body is called the right ventricle)

## Left ventricular blood flow

### Donut-shaped vortex flow forms around the mitral valve

The left and right ventricles have two phases: diastole, when blood is drawn in, and systole, when blood is ejected. During diastole, the mitral valve is released and blood flows into the left ventricle. After the blood enters the left ventricle and turns 180 degrees, the aortic valve is released during systole and the blood is expelled to the rest of the body.

If we trace the flow of blood in more detail, when blood flows in from the mitral valve in the early stages of dilation, symmetrical vortical flows are generated around the anterior and posterior apices of the mitral valve. In fact, when viewed three-dimensionally, a doughnut-shaped vortex flow is formed around the mitral valve. This is called a vortex ring<sup>(2)</sup>

This donut-shaped vortex is formed during the phase of vigorous blood flow into the left ventricle during diastole (rapid inflow phase). In the latter half of the diastole (slow inflow phase), the posterior apex vortex gradually disappears and the anterior apex vortex expands, moving slightly toward the apex. During systole, blood flow is delivered smoothly from this vortex towards the aortic valve.

Vortical flow in the left ventricle in healthy subjects based on blood flow analysis using echocardiography called ultrasound VFM (vector flow mapping).

During systole, we can see that a large clockwise vortex flow occurs and blood is being pumped smoothly from the location of the vortex flow toward the aortic valve. On the other hand, during diastole, blood flow through the mitral valve can be seen to form a doughnut-shaped vortex flow.

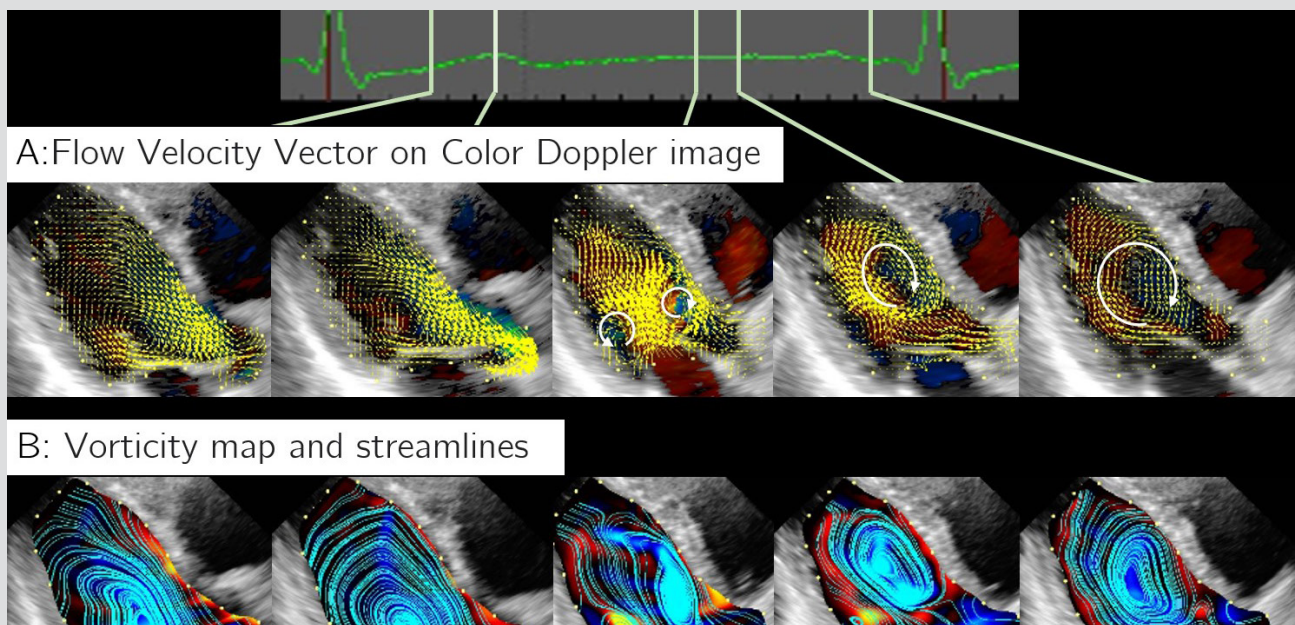


Figure 2 Vortical flow in the left ventricle visualized using ultrasound VFM (vector flow mapping)

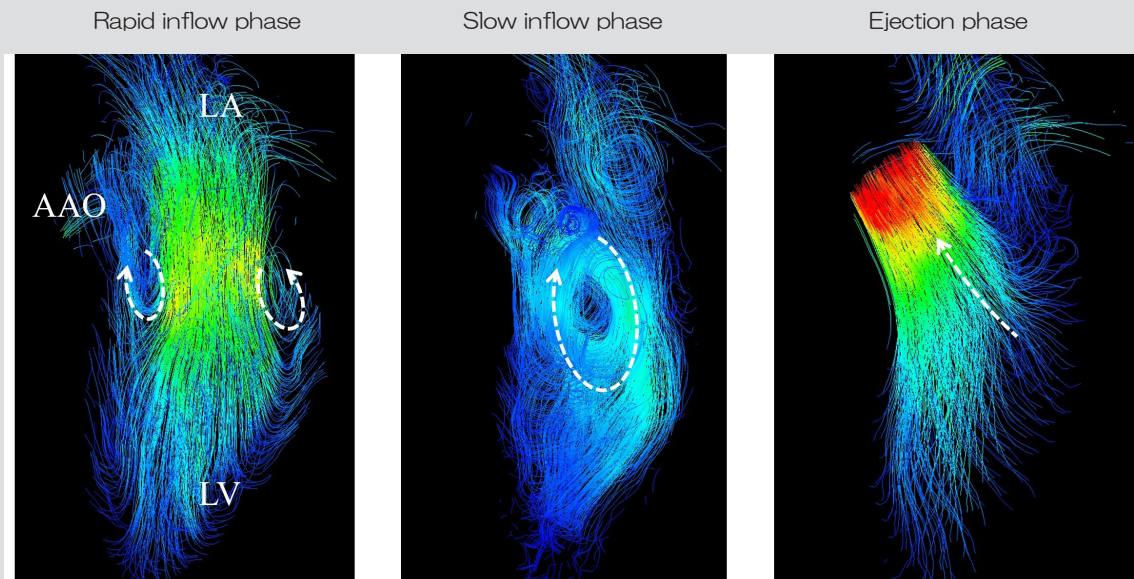


Figure 3 Blood flow in the left ventricle visualized by 4D Flow MRI. Donut-shaped vortex flow can be clearly observed during the inflow phase.

## Left atrial blood flow

### The opening and closing of the mitral valve changes the flow from vortex to linear flow

The left atrium has three roles: reservoir function, conduit function, and booster pump function, which keeps the left ventricle constantly filled with blood while suppressing the pressure increase in the left atrium.

The reservoir function is to maintain inflow by regulating and storing blood volume until the mitral valve opens during the left ventricular systole. The conduit function is the channeling of blood passively from the pulmonary vein into the left ventricle through the mitral valve.

Booster pump function is the function of the left atrium contracting to actively pump blood to the left ventricle.

The slight backflow that occurs at the moment the mitral valve closes collides with the flow of the pulmonary veins on either side, forming a large vortex flow in the atrium, as shown in Figure 4.

Pulmonary venous blood continues to flow in along this vortex flow until the mitral valve opens again. When the mitral valve is opened, the pull from the mitral valve causes the structure of this vortex flow to collapse and change to a linear flow.



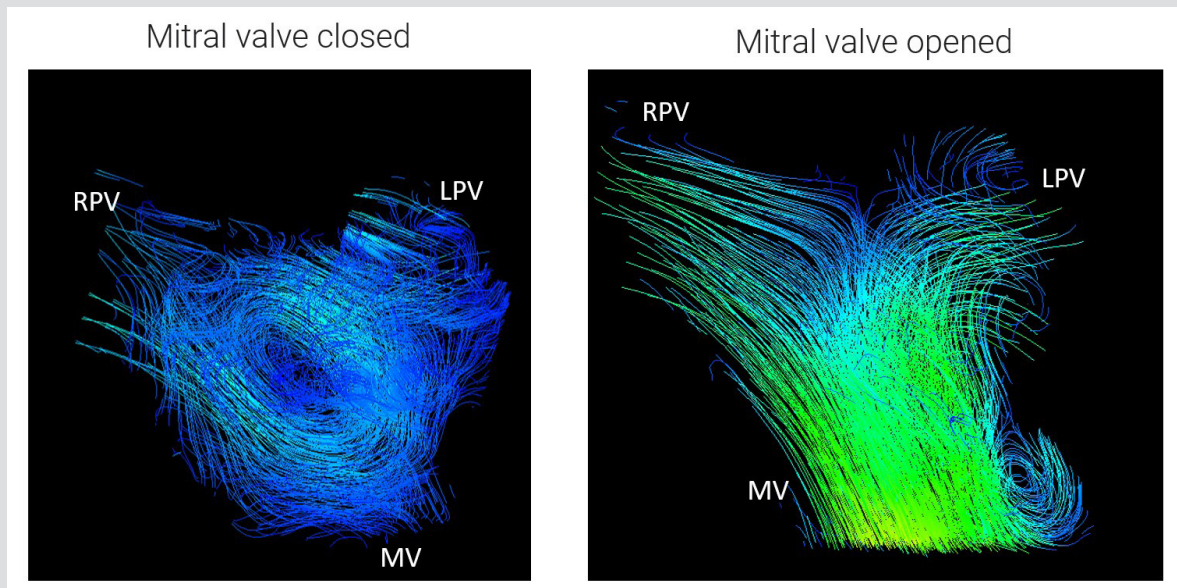


Figure 4 Blood flow in the left atrium visualized by 4D Flow MRI

## Aortic blood flow

### Two vortex currents caused by curvature of the aortic arch.

The aorta is the first tube through which blood pulsed from the left ventricle passes, and it sends the blood flow ejected upwards from the left ventricle to the blood vessels of the lower body via a curve of more than 180 degrees.

In order to receive the large pressure and velocity energy generated by the heart, The aorta has great elasticity, and this elasticity allows systolic pressure to be stored in the blood vessels and gradually flow into the peripheral vessels.

Aortic blood flow is known to often flow in a spiral pattern. This spiral flow is said to be created by the leftward curvature of the aortic arch and the torsional contraction of the left ventricle<sup>(3)</sup>.

Within the sinus of Valsalva, vortex flow occurs along the open valve leaflets. Some reports<sup>(4)</sup> suggest that this vortex flow plays a role in smoothly closing the aortic valve and preventing abnormal stress on the aortic valve during late systole.

Figure 5 shows 4D Flow MRI analysis of blood flow in a healthy subject. In the ascending aorta, secondary flow is small and a linear flow is formed (cross-section 1).

The curve of the aortic arch then gradually creates a secondary flow, with two contrasting vortex flows appearing along the curve (cross-section 2). Such symmetric secondary flows also occur between industrial pipes and are well known as Dean vortices.

Then, as the curve begins to curve backward in three dimensions as well, the secondary flow on one side becomes predominant (cross sections 3-4), leaving only one-directional vortex flow in the descending aorta (cross sections 5-6). During diastole, the secondary flow formed in the aortic arch continues to rotate due to inertia.

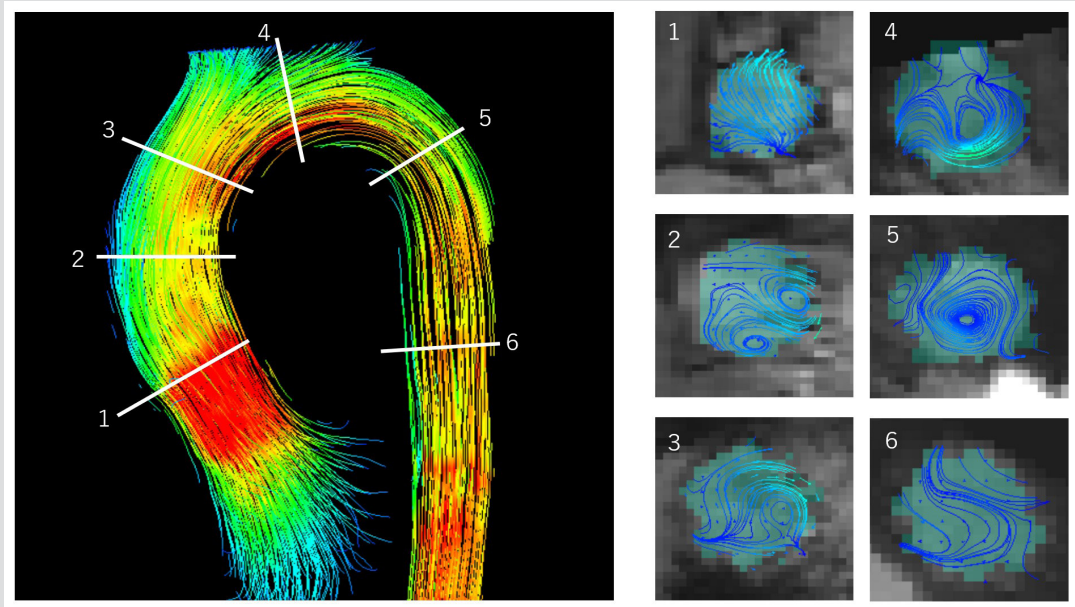


Figure 5 Blood flow in the aorta visualized by 4D Flow MRI

Blood flow in the right atrium and the right ventricle

### Right ventricular system has a characteristic flow that differs from that of the left ventricular system

The right heart system, which is responsible for the pulmonary circulation, flows differently from the left heart system. Within the right atrium, flow from the superior and inferior vena cava merges into a vortex.

During the rapid inflow phase, this force of rotation is maintained and a propulsive force is applied in the direction of the right ventricle, flowing into the right ventricle as a helical flow<sup>(5)</sup>.

Figure 6 shows blood flow in the right heart system of a normal subject. The spiral flow from the right atrium gently flows into the right ventricle by stretching the free wall of the right ventricle forward. During the ejection phase, this spiral structure disappears and the flow is directed straight to the pulmonary artery<sup>(5)</sup>.

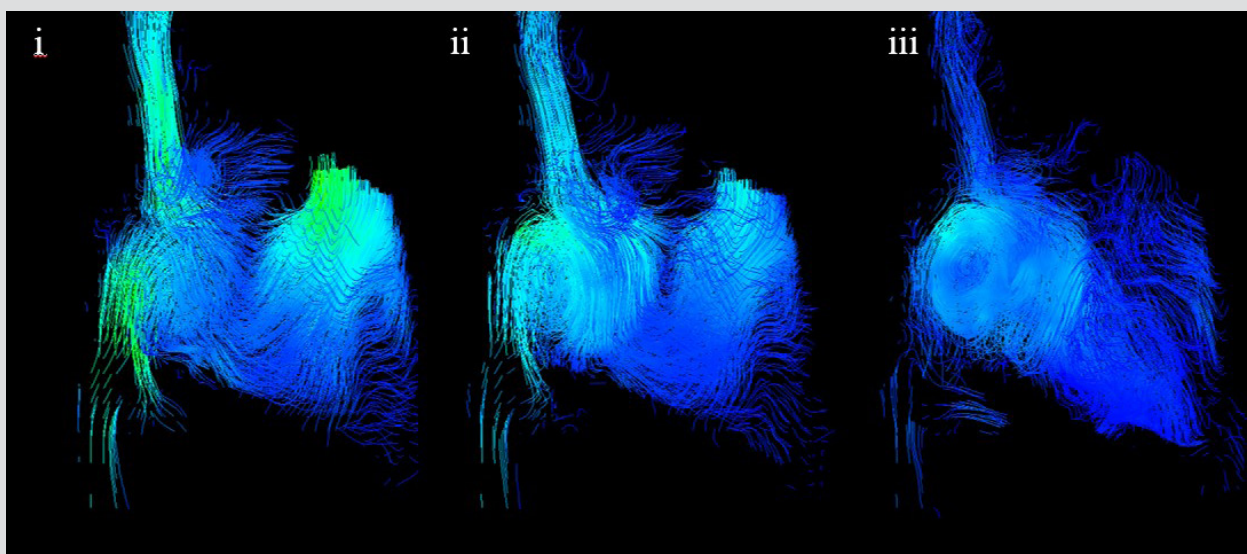


Figure 6 Blood flow in the right atrium and right ventricle visualized by 4D Flow MRI

## Pulmonary artery blood flow

### Angle of bifurcation of left and right pulmonary arteries

The pulmonary artery is the vessel that carries blood from the right ventricle to the lungs. It has a vast capillary bed, exerts only one-tenth the pressure of the arteries of the left ventricle, and is characterized by its thin walls. In addition to the beating of the right ventricle, the expansion of the pulmonary capillary bed due to respiration is said to affect its circulation<sup>(6)</sup>.

In a healthy main pulmonary artery, a straight and less turbulent flow is formed as shown in Figure 7. The pulmonary artery has a smaller curvature than the aorta, resulting in smaller secondary flow and less streamline entanglement.

At the end of the right ventricular systole, the shape of the outflow tract narrows, creating a caliber difference within the main pulmonary artery. As blood flows out of the relatively narrow outflow tract, a difference in blood flow velocity occurs between the major and minor curvatures, causing flow separation and vortical flow.

In pulmonary hypertension, it has been reported that as mean pulmonary arterial pressure increases, vortical flow in the pulmonary artery is significantly formed<sup>(7)</sup> and the duration of residual vortical flow is also increased.

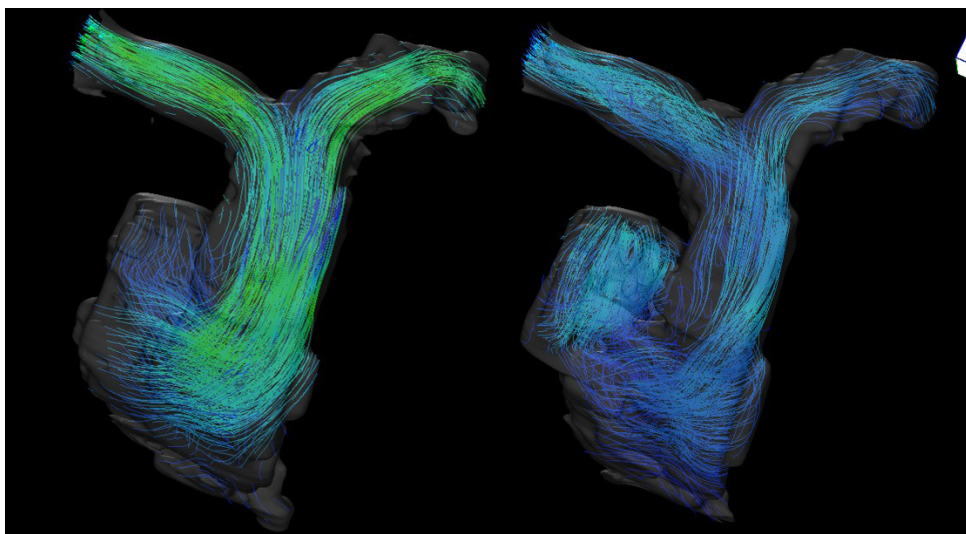


Figure 7 Blood flow in the right ventricle and pulmonary artery visualized by 4D Flow MRI

Because the right pulmonary artery makes a large angle with the main pulmonary artery, blood flow impinging on the bifurcation flows peripherally in a spiral as shown in Figure 8.

On the other hand, the left pulmonary artery does not collide at the bifurcation but flows straight from the main pulmonary artery to the periphery, resulting in a relatively small streamline angle.

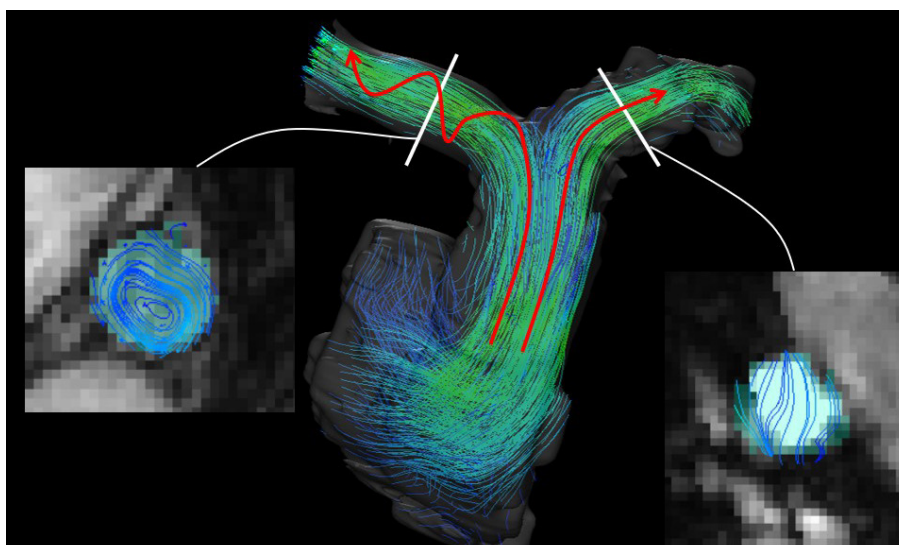


Figure 8: Flow in the bifurcation from the main pulmonary artery to the left and right pulmonary arteries.

The vortex flow varies depending on the angle of the bifurcation.

## Characteristics of left and right heart systems

### The left ventricle is about five times more elastic than the right!

The left ventricle, which performs body circulation, and the right ventricle, which performs pulmonary circulation, have different performance requirements, and their characteristics are expressed in their respective physical property values.

Table 1 summarizes the inertia, elastic force, resistance, and compliance (expandability) at each site.

	Inertia force (blood vessel) [mmHg s <sup>2</sup> /mL]	Elastic force (ventricular) [mmHg/mL]	resistance [mmHg s/L]	Compliance [mL/mmHg]
left ventricle	-	5.480	-	0.182
aorta	18.00	-	198.8	$6.120 \times 10^{-2}$
Micro arteries - capillaries	1.130	-	$3.511 \times 10^3$	$5.350 \times 10^{-3}$
arteriole	0.290	-	322.3	0.310
superior and inferior aorta	4.730	-	82.70	4.079
right ventricle	-	1.300	-	0.769
pulmonary artery	4.120	-	28.40	0.274
pulmonary artery	-	-	416.9	$4.080 \times 10^{-2}$

Table 1: Characteristic values for left- and right-heart systems

The left ventricle turns the incoming blood flow from the mitral valve 180 degrees and directs it to the aortic valve. In other words, a force is required to push the incoming blood flow with large momentum back in the opposite direction. In addition, the body circulation also has large vascular resistance and large inertial force, so a large force is required to circulate it.

In order to efficiently handle such loads, the left ventricular system as a whole has spring-like elasticity and excellent inertia. By storing force in the blood vessels, it can be said that the left ventricular system is able to withstand with large resistance to the circulation.

The right ventricle, in contrast to the left ventricle, is primarily a reservoir. The pulmonary circulation is characterized by much lower vascular resistance and greater compliance than the body circulation. Therefore, it does not have the springiness of the left ventricular system and works primarily to regulate capacity through compliance.



## 2. Turbulence in the heart and blood vessels

### What is turbulence?

### Turbulence occurs everywhere, in water and air.

Turbulence is a condition in which the momentum of the flow (inertia) exceeds the force that restrains the flow (viscosity), resulting in a fine flow associated with the general flow.

Like the smoke from the grilled chicken in Figure 9, turbulence exists everywhere around us. For example, airflow from air conditioners and fans is also turbulent, as is airflow from moving vehicles such as automobiles.

As the tap is gradually turned on, the flow, which was straight at first, becomes turbulent on the surface. The flow, which was laminar with a low velocity, shifts to turbulent flow.

In blood vessels, accelerated blood flow is said to be turbulent in valvular and stenotic lesions. Even in healthy circulations. Systolic aortic blood flow is thought to be turbulent.



Figure 9: Turbulence can be seen in a cooking.

### Advantages of turbulence

### Effective in efficiently mixing fluids.

When turbulence occurs in the blood vessels, more energy is needed to transport the blood. This can result in a strain on the heart.

Turbulence causes some of the pressure and velocity energy of blood flow to be converted into heat, vibration, and noise, which is a disadvantage for the efficient transport of blood. The noise produced by aortic stenosis is thought to be due to turbulence.

However, turbulence is not only a disadvantage. Turbulence also has a role in helping fluids mix. A familiar example is when you dissolve sugar in coffee and mix it with a spoon, you are using the mixing action of turbulence to homogenize the mixture.

In vivo, it has been reported that the mixing action of turbulence promotes diffusion around red blood cells, resulting in efficient oxygen exchange.

Another effect of turbulence is that in catheter contrast, the contrast agent diffuses and homogenizes in a short period of time.

As shown in Figure 10, turbulence also has the effect of efficiently mixing the blood flowing from one organ with the blood flowing to the left or right outlet.

Other studies have been reported that have been tied to turbulence in a variety of phenomena.

Kameneva et al. reported that the greater the degree of turbulence, the greater the amount of hemolysis in assisted circulation such as artificial valves and artificial hearts <sup>(8)</sup>. Nakahara et al. also reported that turbulent flow in lesions not associated with prostheses does not cause hemolysis <sup>(9)</sup>.

On the other hand, regarding endothelial turnover, Davies et al. reported that shear stress due to turbulence promotes DNA synthesis and endothelial cell turnover <sup>(10)</sup>.

Regarding platelets, Ito et al. reported that megakaryocytes sense turbulence, suggesting that platelet production is taking place <sup>(11)</sup>.

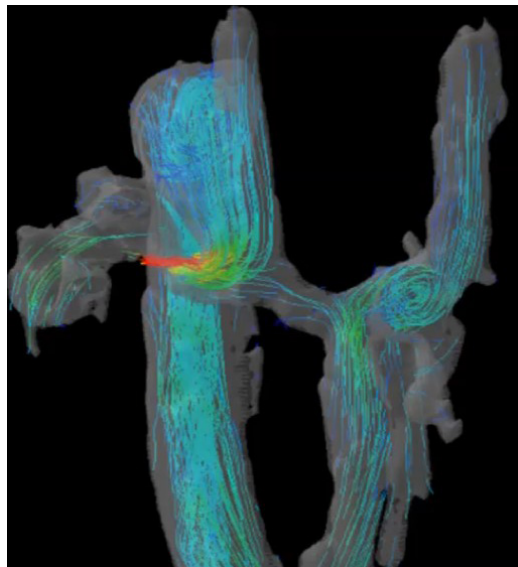


Figure 10 Fontan circulation visualized by 4D Flow MRI

It can be seen that turbulence has a role in mixing the hepatic factor.

What is Reynolds number?

### Evaluates the degree of turbulence based on the balance of inertia and viscosity

Turbulence occurs because the momentum of the flow (inertia) exceeds the force that restrains the flow (viscosity).

The Reynolds number is an index of the degree of turbulence based on the balance of inertia and viscosity. The denominator represents viscosity and the numerator represents inertia.

$$Re = \frac{\rho UL}{\mu}$$

Inertia  
Blood density, velocity, and diameter of the vessel  
Viscosity

It is known that the larger the inertia compared to the viscosity, the larger the Reynolds number and the more turbulent the flow becomes at around 2000 to 2300.

Figure 11 shows the Reynolds number of blood entering the aorta. It easily exceeds 2300 during systole, when the velocity increases. On the other hand, during diastole, the value is close to 0 due to the slow velocity.

The Reynolds number is an indicator that globally determines whether the entire flow field is turbulent or laminar.

In reality, turbulence is caused by a combination of factors, including wall properties and structures. For example, valve cusps in the aorta are obstructions in blood flow and are one source of turbulence.

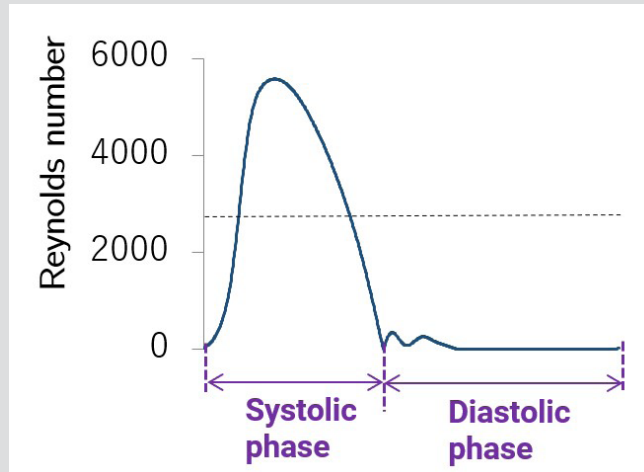


Figure 11: Reynolds number in the aorta. 2000 during left ventricular systole.

exceeds and enters turbulent watersheds, and is close to zero during the dilation phase.

## Mechanism of vortex flow generation

### Vortex flow is generated by the difference in velocity of the flow

Turbulence consists of eddies. Vortices of various sizes are generated in turbulence, and the higher the turbulence energy, the smaller the vortices.

This is because, due to the viscosity possessed by the fluid, under a certain energy, vortex flow below a certain size will be transformed into heat and disappear.

The size of this eddy is called the "Kolmogorov scale" and is one of the indicators when simulating turbulence.

The size of the eddies created by turbulent flow, such as in the aorta, is much smaller than the resolution of MRI or ultrasound, and therefore cannot be seen in real measurements. Even in simulations, calculating turbulent eddies directly (Direct Numerical Simulation: DNS) is very expensive. Since it is difficult to calculate even with a supercomputer, efforts are made to model eddies of a certain size or smaller (turbulence model) to eliminate the need for calculations.

It is the "velocity difference" that causes vortex flow. When a wall or obstacle causes a difference in velocity in the flow, it causes the flow to be turbulent.

Figure 12 is a schematic example of this. Suddenly exiting into a wider pipe diameter creates a velocity difference in space, resulting in a vortex as depicted on the left and right.

Within the heart and blood vessels, vortices with the same structure appear with each beat. These are all caused by differences in velocity.

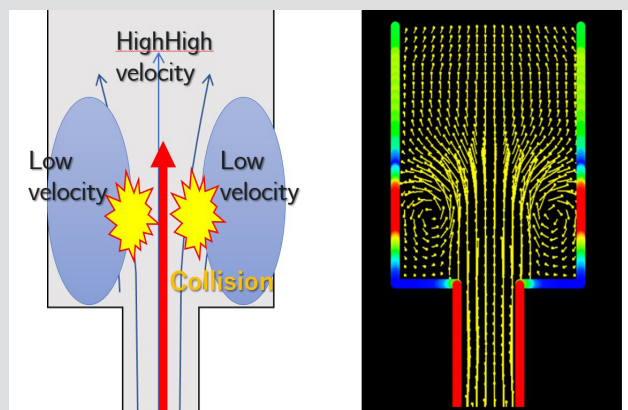


Figure 12: Where the pipe diameter changes abruptly,

vortices are generated due to the resulting velocity difference

### 3. Relationship between blood pressure and blood flow

What is the pressure range?

#### Friction of blood caused by turbulence puts a strain on the heart.

To flow blood with large viscosity through the blood vessels requires a driving force large enough to overcome friction.

The driving force is the blood pressure that the heartbeat exerts on the bloodstream. Blood pressure is the energy that the blood flow contains. Pressure is consumed little by little until it reaches the periphery, where it is reduced.

Normally, the pressure gradient at the valve and aorta is slight. However, as shown in Figure 13, when a pressure gradient occurs, such as in aortic valve disease, the left ventricle must generate extra energy to compensate for the increased load.

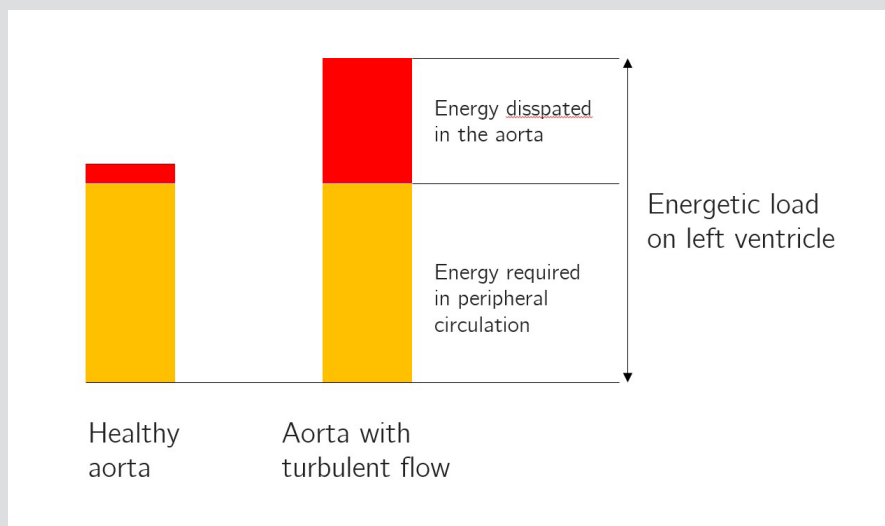


Figure 13: Extra pressure gradient due to aortic turbulence increases the load on the left ventricle

The cause of the pressure differential is "blood friction." When viscous blood rubs against each other, pressure energy is converted to heat and sound, resulting in loss of pressure energy.

Since friction is caused by the velocity difference in blood flow, eddies and turbulence are closely related to pressure drop.

Next, let's look at the flow of each cause of energy loss.



## (1) Energy loss caused by stenosis

The severity of a stenotic lesion is assessed by the pressure gradient. It is commonly expressed as  $4v^2$  based on the velocity of accelerated blood flow, but even with the same stenosis rate and the same blood flow velocity, the pressure gradient can be different. In such cases, fluid analysis can be used to calculate an accurate pressure gradient.

For example, in the case of a tubular stenosis and a tapered stenosis as shown in Figure 14, the tubular stenosis has greater resistance and a larger pressure gradient than the tapered stenosis, even if they have the same stenosis rate. This is due to turbulent flow with separation before and after the stenosis and greater shear stress with the wall at the stenosis<sup>(12)</sup>.

### What is total pressure?

It is the sum of "static pressure" and "kinetic pressure," which are pressures (strictly speaking, relative pressure values), and is said to refer to the potential energy of a flow.

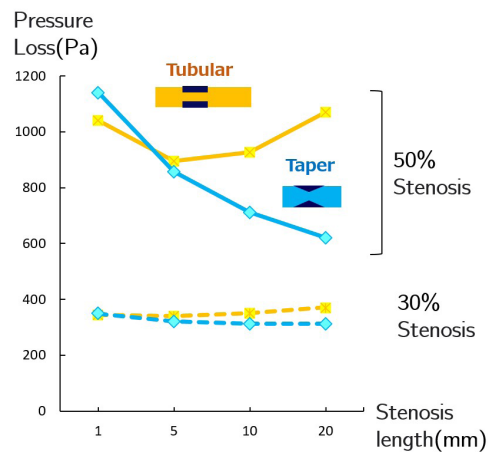


Figure 14: Change in pressure range due to different shapes of stenosis  
(top: tubular, bottom: tapered)

Figure 15 shows the total pressure loss by two stenosis types. Tubular type has a larger pressure range at the stenosis.

Energy loss also depends on the length of the constriction. In the case of a tapered type, if the constriction ratio is the same, the longer and gentler the tapered portion is, the less likely flow separation is to occur, and thus the pressure loss is smaller<sup>(12)</sup>.

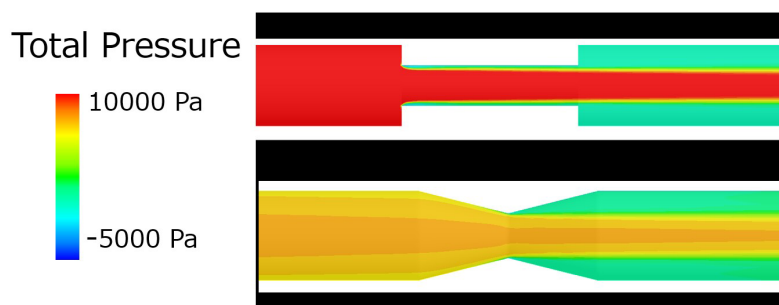


Figure 15 shows the total pressure loss by two stenosis types.  
Tubular type has a larger pressure range at the stenosis.

## (2) Energy loss caused by impingement on vessel wall

When blood flow impinges on a wall, pressure loss also occurs due to friction between the wall and the blood flow, and the resulting turbulence.

Figure 16 Visualization of accelerated blood flow in aortic valve stenosis and flow separation. Accelerated blood flow can be seen impinging on the wall of the ascending aorta, creating a vortex flow.

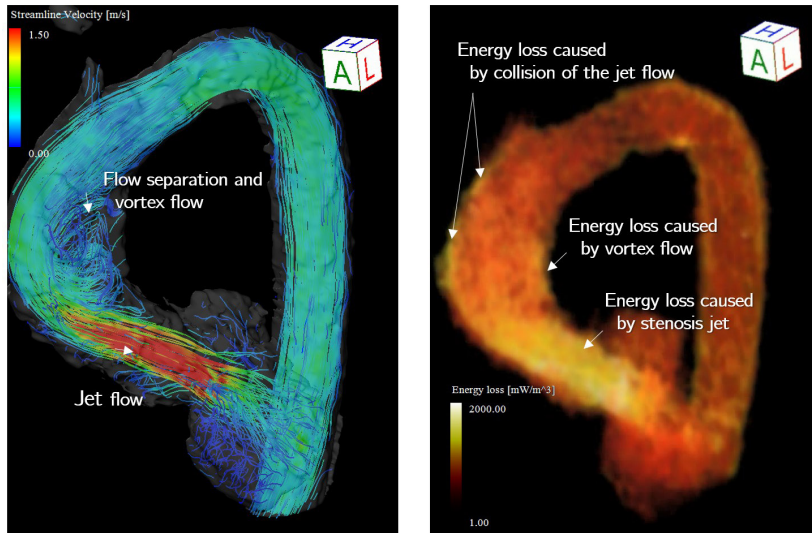


Figure 16: Blood flow collides with a wall and significant energy loss occurs

## (3) Energy loss caused by vascular bending

Sudden bending of blood vessels can also cause pressure loss as the blood flow impinges on the walls, creating turbulence.

Figure 17 shows the results of an investigation of the relationship between centerline curvature and energy loss; the Energy Loss Index (ELI) is an index of energy loss divided by body surface area.

The results suggest that sharp curves disrupt the flow and increase losses<sup>(13)</sup>.

### $\curvearrowright$ Curvature

Quantity representing the degree of curvature of a curve or curved surface

For example, the curvature of a circumference of radius  $r$  is  $1/r$ . The tighter the bend, the greater the curvature.

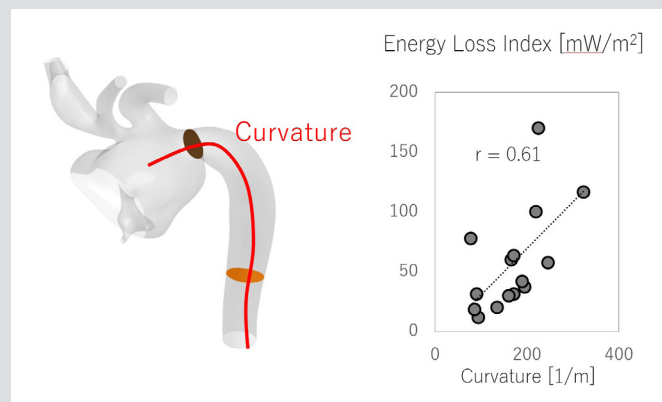


Figure 17 Report comparing Energy Loss Index (ELI) and aortic arch curvature in reconstructed aorta.

## Static and dynamic pressure of fluid

### Static pressure is converted to dynamic pressure at vascular stenoses.

There are two types of pressure that a fluid has: static pressure and dynamic pressure. It is static pressure that is measured as the pressure felt when standing still in water or as blood pressure, as shown in Figure 18. Static pressure is the pressure exerted in a stationary fluid.

Dynamic pressure, on the other hand, is the force being pushed from the flow. For example, a hand out of a car window or a force pushing in a river as shown in Figure 19 is dynamic pressure.

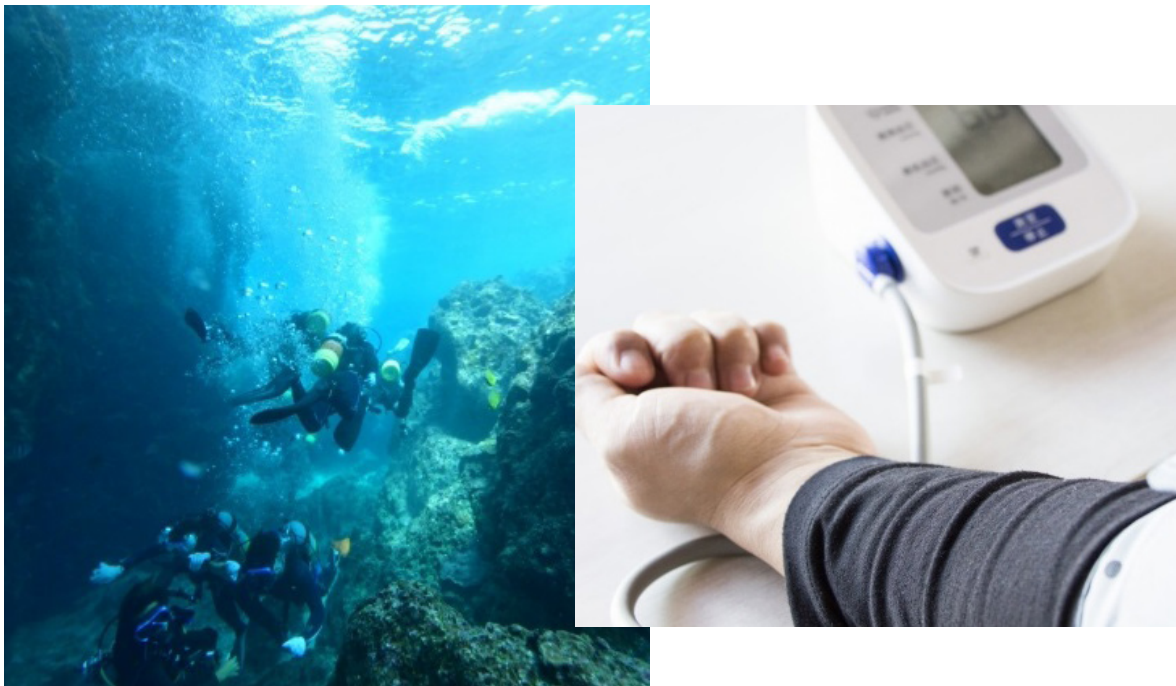


Figure 18 Example of static pressure

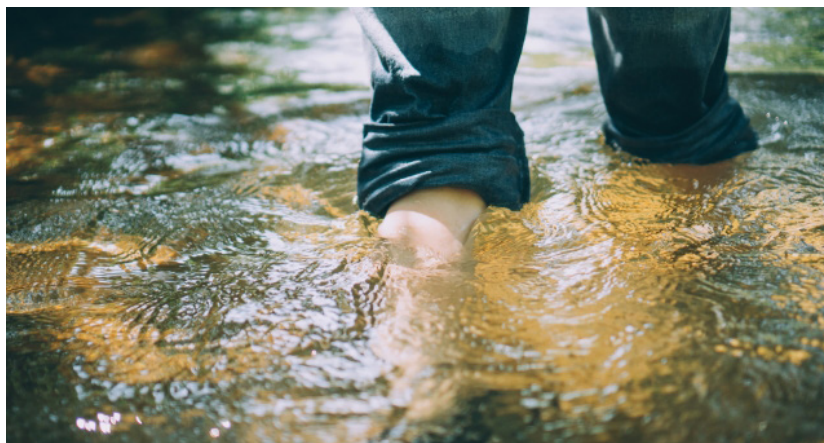


Figure 19: Example of dynamic pressure

Dynamic and static pressures are converted to each other in the flow. A schematic diagram of the site of stenosis and the location of conversion is shown in Figure 20.

For example, when there is a stenosis of a blood vessel, the static pressure decreases at the center of the stenosis, and the decreased static pressure is converted to dynamic pressure.

If there is no energy loss due to viscosity, the sum of static and dynamic pressures remains constant, and after the stenosis is released, the static pressure recovers to the same level as before the stenosis. This phenomenon is called "pressure recovery."

In real-world flow, blood pressure is lower after a stenosis because of energy loss due to collisions and turbulence in a jet flow caused by the stenosis.

### Bernoulli's principle (Bernoulli's theorem)

A theorem that states that when energy loss or supply is negligible in a given flow, the energy at two points on a single streamline is equal (conserved).

It is valid for a perfect fluid, which is a fluid without viscosity.

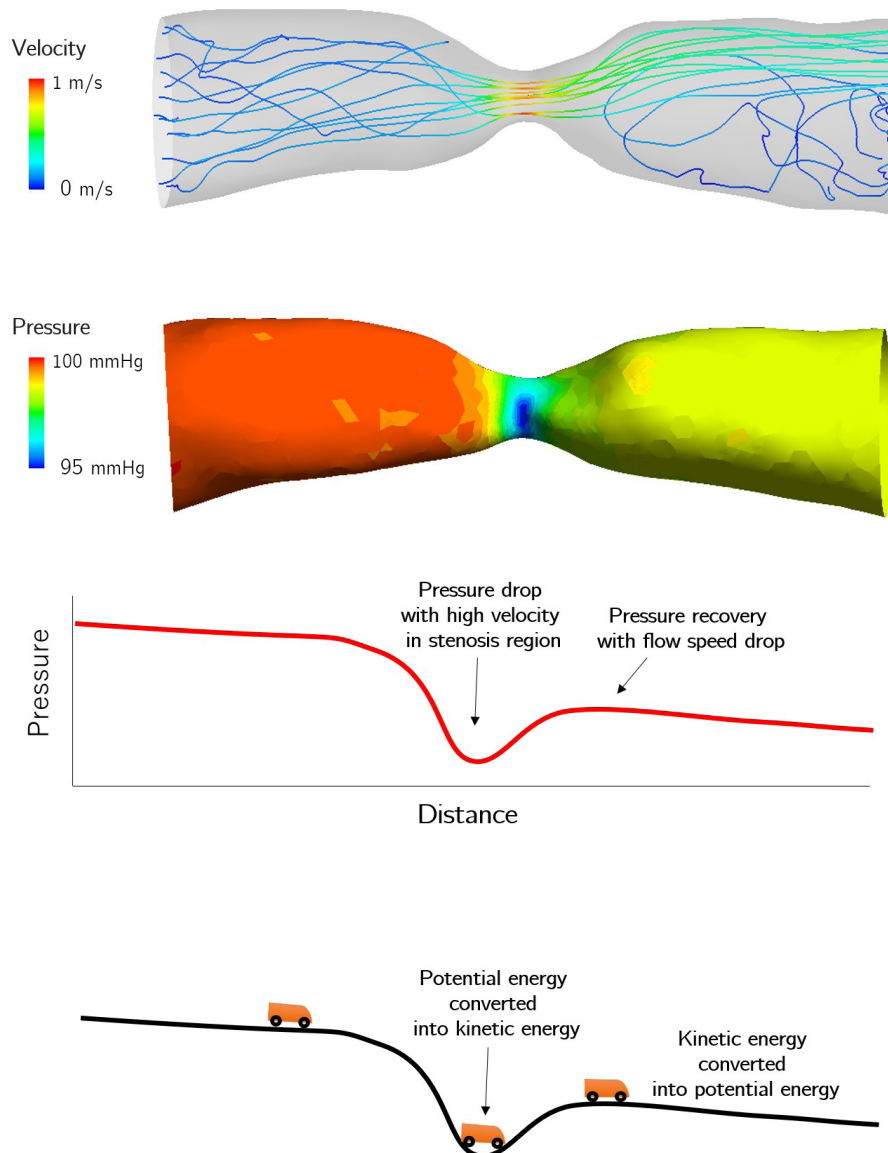


Figure 20: Static and dynamic pressures flow while being converted into each other



# Chapter 2: Methods of Blood Flow Analysis

## 1. Three methods of blood flow analysis

This chapter introduces three analysis methods: Computational Fluid Dynamics (CFD), 4D Flow MRI, and Ultrasonic Vector Flow Mapping (VFM).

All of them can observe streamlines, energy loss, WSS (Wall Shear Stress), and OSI (Oscillatory Index). However, 4D Flow MRI and ultrasound VFM are less accurate for WSS.

Table 2 shows a comparison of the three methods. See also the data required for the analysis.

Table 2: Comparison among modalities

	CFD	4D Flow MRI	Vector Flow Mapping
Principles of blood flow measurement	Computer simulation	Phase contrast method,	Color Doppler method
Indicated site* <sup>1</sup>	Coronary artery, Aorta, Vena cava, Pulmonary artery, Cerebral artery, etc.	Coronary artery, Aorta, Vena cava, Pulmonary artery, Cerebral artery, Atrium, Ventricle, Valve, etc.	Left ventricle, Ascending aorta, Pulmonary artery, Carotid artery, etc.

\*1 : Analysis of vessels other than those indicated above may also be possible.

## 2. Computational fluid dynamics (CFD)

### Simulation of fluid flow

Computational Fluid Dynamics (CFD) is a technique for simulating fluid flow on a computer.

In this method, a geometry for the fluid domain is created on a computer and fluid equations are solved in the domain.

### Strengths and Cautions

Since CFD is calculated iteratively to minimize numerical errors, numerical errors are smaller compared to experiments and measurements.

In addition, it provides high spatial and temporal resolution to solve complex problems.

### Application Examples

CFD was first used in weather forecasting in the 1940s and has been widely used industrially. Since then, computer performance has improved dramatically, and various practical calculation methods have been devised, making CFD now an extremely powerful tool for understanding the flow of materials.

Figure 21 shows an example of application in aircraft. By changing the aircraft design and conducting CFD analysis, efforts are being made to suppress the vortex behind the fuselage, which is the dominant factor in aerodynamic drag.

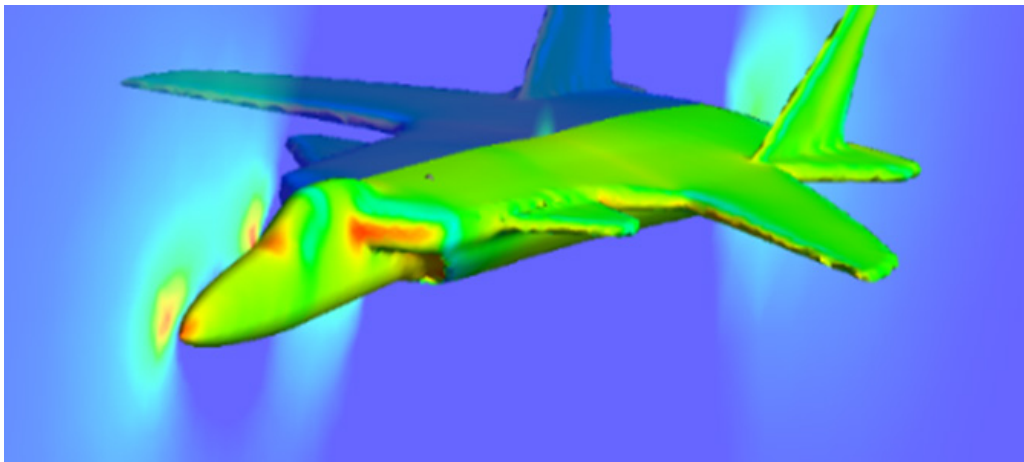


Figure 21: Industrial applications of CFD.

Visualization of pressure gradients around the aircraft

CFD is indispensable in a variety of industries, as simulations can be used to analyze systems that are difficult to analyze in reality, such as highly hazardous or time-consuming experiments.

In recent years, CFD is expected to be useful not only in the industrial field but also in the medical field.

## Data Necessary for Analysts

### Data required for analysis

The following conditions are required for CFD analysis of vascular systems

- Geometry of blood vessels
- Physical properties of blood
- Boundary conditions  
(flow rate, pressure, and other conditions on the entrance and exit of the geometry)

For geometry, CT and MRI are often used to acquire the shape of blood vessels.

Next, blood physical property values are applied to general conditions unless they are extreme cases, although the properties of blood (e.g., viscosity) will differ depending on the medical condition.

Finally, boundary conditions are very important to accurately calculate the characteristics of the biological flow. Boundary conditions are given as the blood flow velocity or pressure exerted on the inlet/outlet of the vessel being analyzed. Since it is an important factor that determines patient-specific information, modeling is mainly based on ultrasound, MRI, catheter, and other measurement data.

## 3. 4D Flow MRI

### 3D blood flow information in real time

Actual measurement of blood flow information in 3D space

MRI-based blood flow measurement techniques have developed to date, starting with the technique for measuring blood flow velocity distribution using an imaging method called phase contrast.

Among them, the imaging technique that provides three-dimensional blood flow information with time variation is called 3D Cine PC MRI or 4D flow MRI, and is used to study blood flow dynamics, such as aortic diseases<sup>(14)–(16)</sup>.

Figure 22 shows a computer visualization<sup>(17)</sup> of the blood flow velocity data output by this imaging method. Streamlines and other features can be used to better understand the actual measured blood flow field.

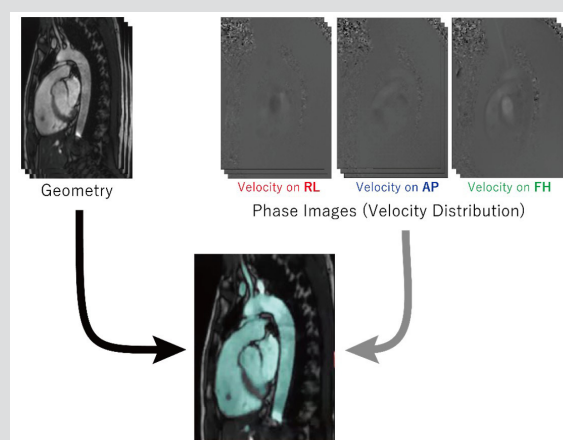


Figure 22 Shape information obtained from MRI (top left) and flow velocity components in three directions (top right), and the applicable area determined by combining these (bottom). Such data can be acquired and constructed over time.

## Strengths and Cautions

MRI is the only examination method that can non-invasively measure actual blood flow velocity distribution in three-dimensional space, and computer graphics can be used to display the results for a specific purpose.

On the other hand, 4D flow MRI takes images in 3D space over time, so the imaging time is long and sufficient resolution cannot be obtained in many cases.

However, recent improvements in the performance of MRI systems and the emergence of new imaging methods have dramatically increased speed, raising expectations for clinical applications.

### Data Necessary for Analysts

## Data required for analysis

In the case of blood flow analysis with MRI, since the obtained velocity field is visualized, it is not necessary to set up the physical properties of the blood or the computational conditions as in CFD.

As shown in Figure 22, if information on the velocity components in three directions (RL, AP, and FH directions) is available, a vector can be created. Cine images may also be used to identify the shape of the vessel, since it is not possible to determine where the flow is by itself.

## 4. Ultrasonic measurement

### Calculate internal pressure range from measured data

Ultrasound measurements use ultrasound PIV (Particle Image Velocimetry), which measures blood flow based on the motion of contrast agent particles. New methods such as VFM (Vector Flow Mapping) and IVPD (Intra Ventricular Pressure Difference), which calculate blood flow velocity in the direction perpendicular to the beam using physical equations as shown in Figure 23, have also emerged, bringing a new perspective to cardiovascular care.

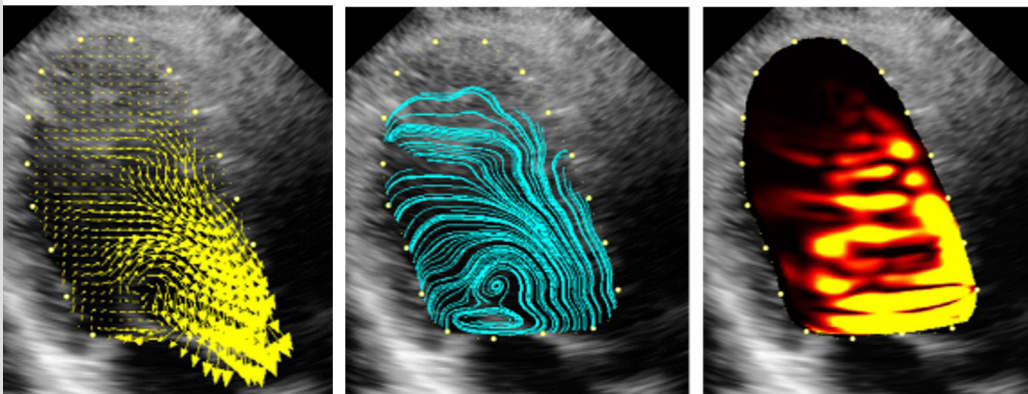


Figure 23 Velocity vectors (left), streamlines (center) and energy loss (right) in the left ventricle visualized by VFM.

The ability to calculate blood velocities in the direction perpendicular to the beam has made this visualization possible

## Strengths and Cautions

Ultrasonography is noninvasive and can be applied to outpatients. Blood flow analysis using ultrasonography is a clinically very easy method of blood flow analysis, with little time and computational burden.

On the other hand, since the observation range is limited to two dimensions, correct evaluation is not possible unless the flow of the object to be analyzed is in the two-dimensional cross section.

For example, if the core of the jet of valve stenosis deviates from the cross-section, it can lead to underestimation of energy loss, etc. It is also difficult to evaluate vortices that occur in the depth direction. To cope with this problem, a three-dimensional VFM is currently being developed<sup>(17)</sup>, and future developments can be expected.

## Application Examples

From an ultrasound color M-mode image of the apex of the heart, the Intraventricular Pressure Difference (IVPD) can be calculated by solving Euler's equation, as shown in Figure 24. This is a technique that has attracted much attention in the study of the pathogenesis of cardiac diastolic failure.

Commonly used indices of left ventricular distensibility are the mitral flow velocity pattern (TMF) and pulmonary venous flow velocity pattern (PVF).

However, a deeper understanding of myocardial performance requires separating the ability of the left ventricle to actively expand by expending energy from its softness to receive blood as it then passively expands.

Calculating IVPD makes it possible to map the force with which the left ventricle actively draws blood by measuring the pressure gradient along the long axis of the left ventricle. It is possible to assess which parts of the myocardium are drawing blood flow and with what degree of force.

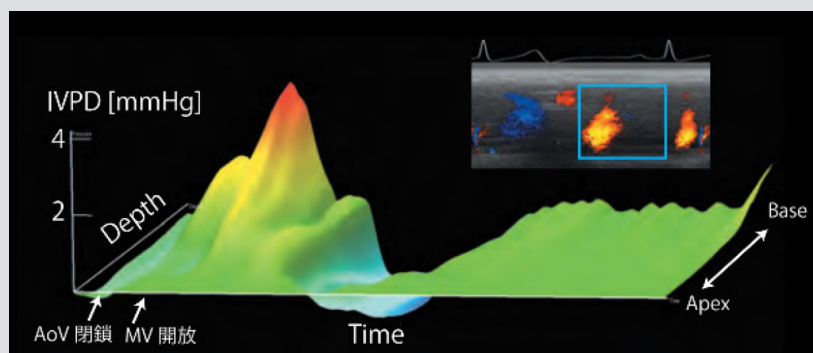


Figure 24: Pressure gradient in the left ventricle calculated from ultrasound color M-mode.

The horizontal axis indicates time, and the depth direction is from apex to base of the heart, and the longitudinal axis represents the pressure range with the apex as the base axis.

### Data Necessary for Analysts

## Data required for analysis

Ultrasound measurement, like MRI, is an analytical technique that visualizes blood flow from measured data.

In addition, the velocity field in a two-dimensional plane is calculated in software using the velocity information on the beam and the wall motion obtained by speckle tracking. In this case, only a color Doppler image is required.



# Chapter 3: Examples of Blood Flow Analysis

Here we will introduce some papers on blood flow analysis and what kind of analysis has been achieved in what cases.

Many people who are just getting started with blood flow analysis may think that they already have a case in mind, but are not sure what they can do.

We hope that by reading this chapter, you will find seeds for your research, such as "Let's apply this method of analysis to our own cases," or "This paper discusses this, but if we look at it from this perspective, we may be able to consider it differently."

## 1. Virtual surgery simulation

(Valsalva aneurysm)<sup>(18)</sup>

### Blood flow analysis reveals problems

The case presented here is a patient who underwent right coronary artery-right atrial fistula closure surgery at the age of 3 years, had a stroke at the age of 18 years, and was diagnosed with a valsalva aneurysm and fistula remnant short circuit with no sequelae.

The left side of Figure 25 shows the 3D geometry constructed from CT and the right side shows the results of CFD (Computational Fluid Dynamics) simulation. The simulation results show that a vortex flow is formed in the mass, and the flow velocity is low throughout one heartbeat. In addition, the direction of the wall shear stress (WSS) is not stable due to the vortex flow, resulting in a high Oscillatory Index (OSI) value.

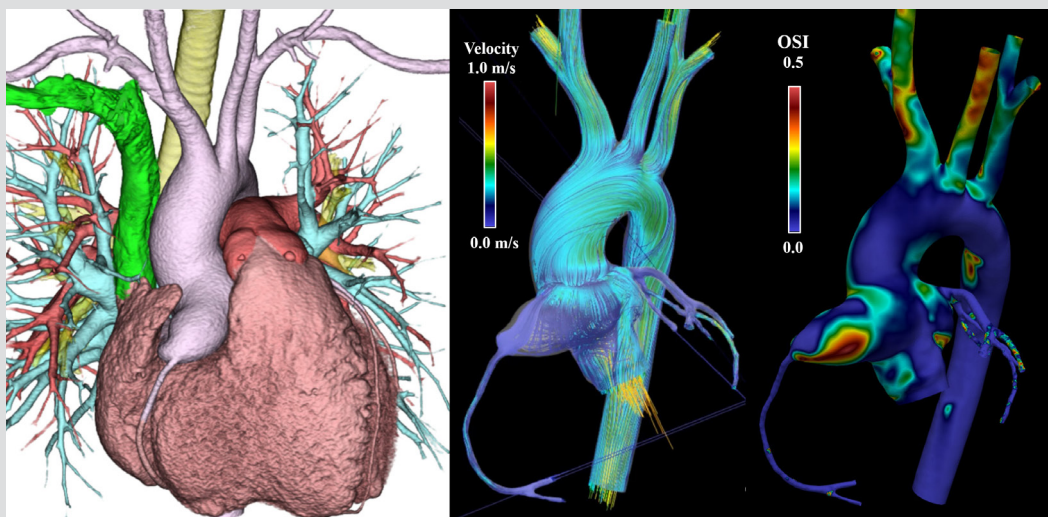


Figure 25 Preoperative blood flow visualizes turbulence within a coronary artery aneurysm and stress inside the coronary artery aneurysm.

High OSI has been suggested to produce ROS in the vascular endothelium, leading to endothelial damage

### Virtual surgery selected for artificial vascular reconstruction

Blood flow was compared in the simulation with virtual aortic root replacement + 6 mm artificial vessel right coronary artery reconstruction aortic root partial replacement + right coronary artery bypass. There was no stagnation in either case.

No problems were observed in OSI. In addition, right coronary artery flow rates were 71 mL/min preoperatively, 70 mL/min with 6 mm prosthesis, and 75 mL/min with bypass, all of which were predicted to provide adequate blood flow.

Since there were no problems with either surgical strategy in terms of blood flow, reconstruction with a 6 mm artificial vessel was chosen to avoid the risk of using a vein graft. Because the Valsalva aneurysm was fused to the right ventricular outflow tract, it was closed within the aneurysm, the fistula inlet was closed, and the right coronary artery was reconstructed with a 6 mm artificial vessel.

## 2. Blood flow analysis to determine treatment guidelines

### Pulmonary valve regurgitation after TOF surgery<sup>(19)</sup>

#### Integrated data from 4D Flow MRI

4D Flow MRI can measure the degree of accelerated blood flow in outflow tract stenosis, the degree of regurgitation, ventricular volume, and the excess cardiac load (energy loss) due to accelerated blood flow and regurgitation. 4D Flow MRI alone has the potential to determine the overall pathology.

The case report presented here describes a case of pulmonary valve regurgitation after endocardial repair of tetralogy of Fallot (TOF) in which 4D Flow MRI was used to select a treatment strategy. 4D Flow MRI measured regurgitation rate, energy loss, and ventricular volume, which guided the decision to perform pulmonary valve replacement.

The left flow line in Figure 26 shows diastolic regurgitation visualized by 4D Flow MRI. This regurgitation can also be quantified as shown in the lower right graph, and in this case the regurgitation rate was as large as 67.7%, suggesting that the right ventricle was capacitively loaded.

Figure 26 right visualizes the magnitude of energy loss caused by turbulence, with bright areas indicating areas of high energy loss. In this case, 4D Flow MRI showed that turbulence in the pulmonary artery during systole and valve regurgitation during diastole caused very large energy loss (7.62 mW, approximately 8 times normal).

The volume of the right ventricle was also evaluated in systole and diastole, respectively, and the large end-diastolic and end-systolic volumes were also considered problematic.

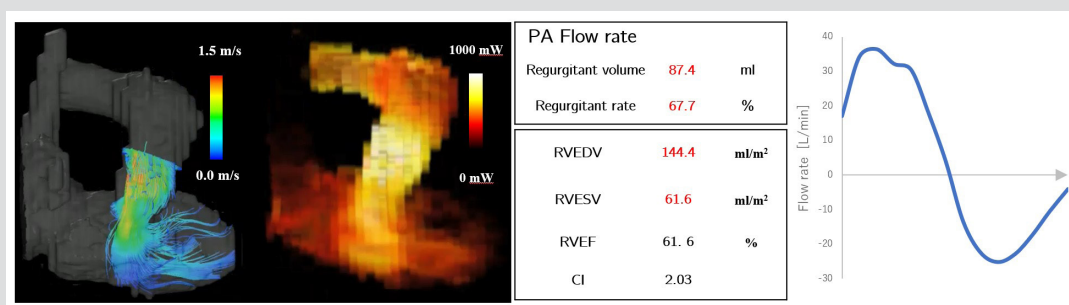


Figure 26: Reverse flow, energy loss, and ventricular volume after endocardial repair of tetralogy of Fallot. The graph on the right shows the flow rate in the reverse flow portion of the figure left.

It represents and quantifies the forward flow in systole (upward convexity) and the reverse flow in diastole (downward convexity part)

### 3. 4D Flow MRI blood flow analysis before and after treatment

(Chronic aortic dissection) <sup>(20)</sup>

#### Actual measurement of blood flow in the false lumen changes over time after TEVAR

Stanford type B aortic dissection has recently been treated with stent graft interposition (TEVAR). This treatment blocks the entry site and prevents blood from flowing into the false lumen, promoting vascular remodeling and reducing the size of the false lumen itself.

On the other hand, there have been cases where the entry site was blocked after enlargement, such as an aortic aneurysm, and remodeling did not proceed well, resulting in further enlargement of the false lumen.

Utilizing 4D Flow MRI, it is possible to visualize how blood flows into the false lumen, as shown in Figure 27.

The upper right is an analysis near the entry of the aortic arch. The upper and lower streamlines appear to be divided into two layers, but the upper streamlines are considered to be the false lumen and the lower streamlines are considered to be the true lumen.

Below right is an analysis of the abdominal aorta. The red areas show areas of high blood flow velocity, where blood flow is accelerated in the narrow part of the true lumen, and blood flow is seen flowing into the false lumen from the underlying re-entry.

On the left is an analysis from the aortic arch to the abdominal aorta. Areas such as green and yellow indicate high blood flow velocity, while blue areas indicate low blood flow velocity. You can see that the colors are divided between the true and false lumens.

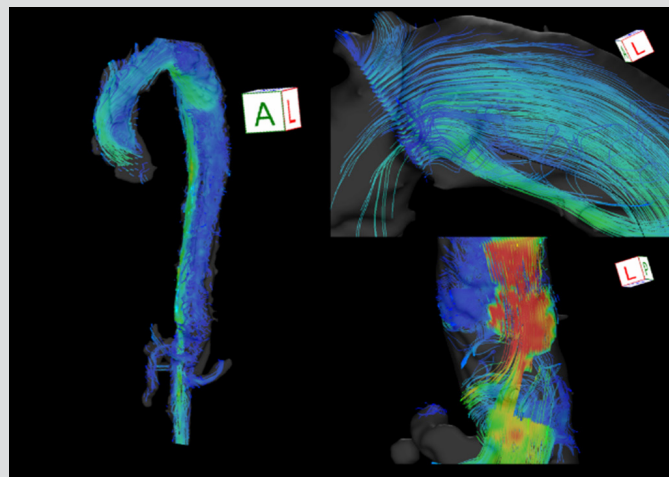


Figure 27 Flow lines in the true and false lumens in aortic dissection cases visualized by 4D Flow MRI

This study utilizes 4D Flow MRI to measure and observe blood flow in the false lumen and reentry area (fissure) under three conditions: preoperative TEVAR, immediate postoperative, and 6 months postoperative to track changes in blood flow over time.

The subject is a 50-year-old man who developed a Stanford B type aortic dissection 6 years ago.

The aortic arch to the descending aorta was enlarged to about 60 mm and was treated with TEVAR.

Preoperatively, it has one entry section and four reentries; postoperatively, it has only three reentries because the first and last two were closed by TEVAR.

Figure 28 shows the volume change with contrast-enhanced CT. It can be seen that the false lumen is slightly larger in volume postoperatively, but then decreases.

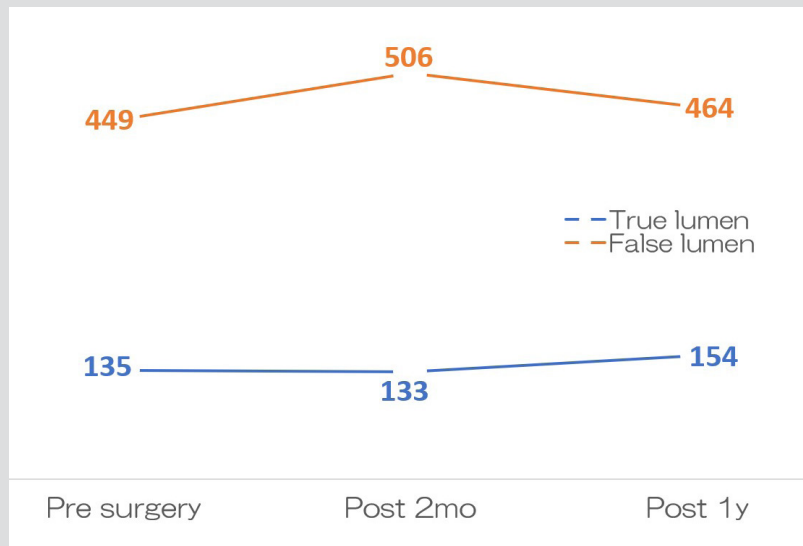


Figure 28 Pre- and post-operative volume changes of vacuum and false cavity

### Primary entry closure significantly changes hemodynamics in the false lumen

Figure 29 shows the blood flow through each entry point and from the true to the false lumen, showing the dynamic changes in the blood flow field due to the closure of the entry points by TEVAR.

Immediately after surgery, Primary entry was the main source of false lumen blood flow, but it gradually disappeared and was replaced by a supply of blood flow from the reentry into the false lumen. After 6 months, however, that increase also ceased, resulting in a decrease in overall blood flow to the TEVAR false lumen.

Intracavitary blood flow was altered preoperatively and postoperatively, with a marked increase in intracavitary blood flow up to the second re-entry site after TEVAR, but the amount of intracavitary blood flow had subsided after 6 months. In other areas, TEVAR resulted in an increase in intratumoral blood flow.

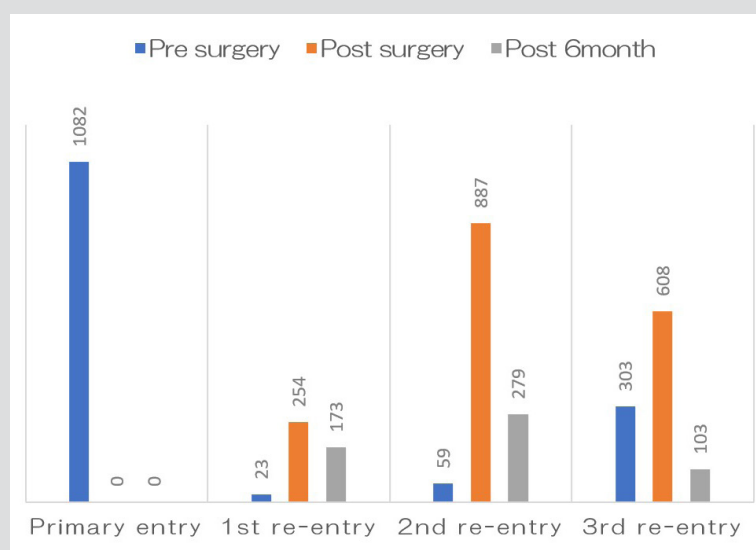


Figure 29: Pre- and postoperative performance of time-averaged blood flow into the entry site (ml/min)

## 4. Surgical design of pulmonary angioplasty

(Congenital heart disease)<sup>(21)</sup>

### Virtual surgery to design the shape of the patch

Pulmonary artery stenosis, with its complex geometry, is difficult to predict postoperatively and is greatly influenced by the skill and experience of the surgeon. By using CFD analysis of virtual surgery, it is possible to predict in advance what the blood flow field will be like on the computer, which is useful for actual surgical strategy.

This study proposes a method to design a better surgical procedure based on fluid dynamics from preoperative CT and incorporate it into design drawings.

Here are the steps

- (1) Create a virtual geometry with the stenosis removed from the preoperative CT.
- (2) Determine the incision line with respect to the original stenosis shape.
- (iii) Take the difference between the vessel diameter of the virtual shape and the original shape, as shown in the virtual shape.

Calculate the shape and size required for the patch to be finished.

Based on the calculated shape and size, the patch is made into a drawing of the actual size table.

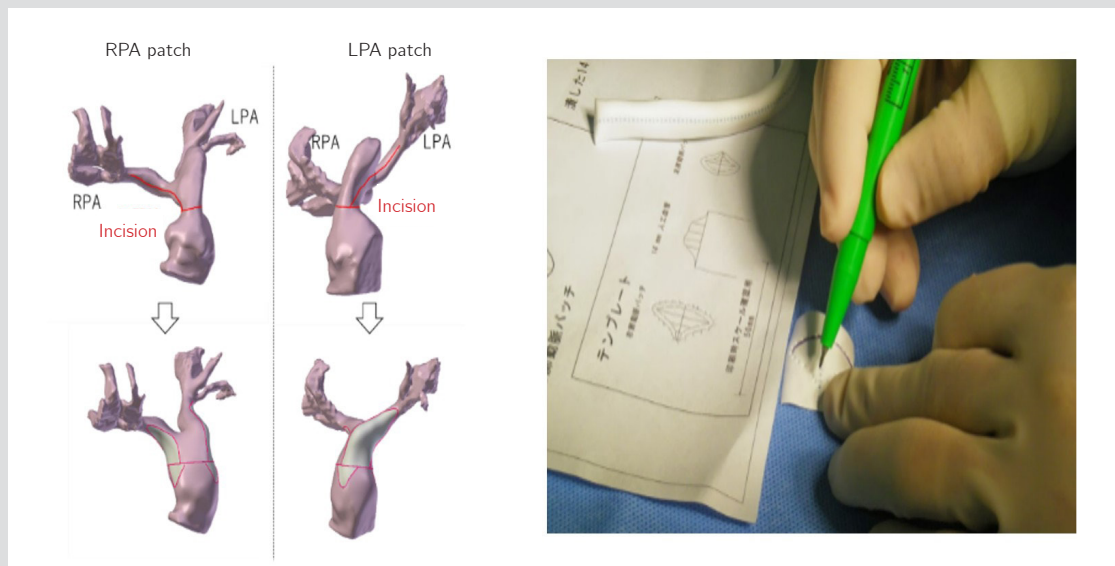


Figure 30: Cutting out a patch from a blueprint

RPA: Right Pulmonary Artery

LPA: Left Pulmonary Artery



## Surgery is performed as simulated

Figure 31 shows the mean and range of values for energy loss (EL) and WSS, respectively, with error bars. Comparing preoperative to virtual surgery and preoperative to postoperative, both EL and WSS decreased significantly. There was also no significant difference between virtual surgery and postoperative.

These results confirm the validity of preoperative CFD evaluation by virtual surgery.

Pulmonary artery angioplasty is a surgery in which the physician's experience and skill are critical, but these virtual surgical simulations are independent of the physician's experience and skill, making it possible to select the ideal procedure for the patient.

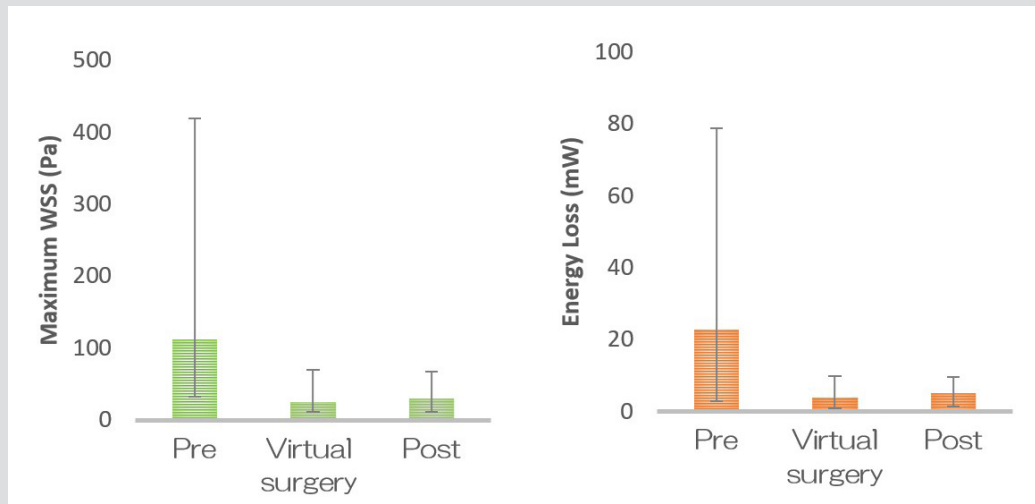


Figure 31 Comparison of EL and WSS for 6 cases preoperatively, hypothetically, and postoperatively  
Error bars indicate a range of values

## 5. Revascularization by aortoplasty

(Congenital heart disease)<sup>(22)</sup>

### Determine aortic reconstructive procedures from ELI and WSS.

The paper presented here is a report on aortic reconstructive surgery for hypoplastic left heart syndrome, in which blood flow was evaluated by CFD and used as a criterion for treatment strategy.

The Norwood procedure for hypoplastic left heart syndrome is a high-risk procedure requiring high skill. Turbulence in the reconstructed aortic arch may increase the cardiac load and worsen cardiac function. To avoid this, aortic arch reconstruction in two stages may be beneficial.

This study focuses on "efficient blood flow" and aims to develop a protocol to determine if a second stage of aortic arch reconstruction is necessary by evaluating the energy loss index (ELI = energy loss/body surface area) and WSS in the aortic arch with CFD.

From the average of the analysis of 5 cases without aortic problems (ELI: 42.2 a 16.8 mW/m<sup>2</sup> , WSS: 97.5 a 27.3 Pa), the protocol in Figure 32 was developed.

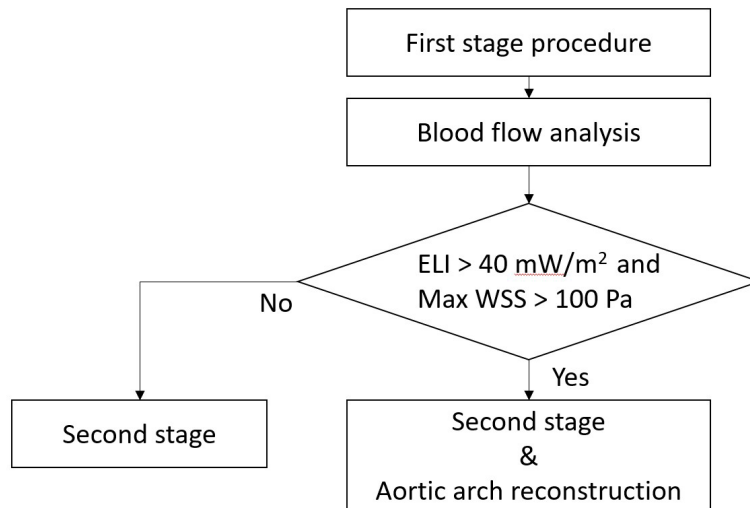


Figure 32: Reference values created from the average ELI and WSS values of the five cases.

## Virtual surgery to confirm pre- and post-operative changes

Figure 33 shows a graph comparing the maximum energy loss and WSS before, virtual surgery, and after surgery. It can be seen that both are significantly reduced by reconstruction, and at the same time, they serve well as a predictive analysis, as there is no significant difference between virtual surgery and postoperative surgery.

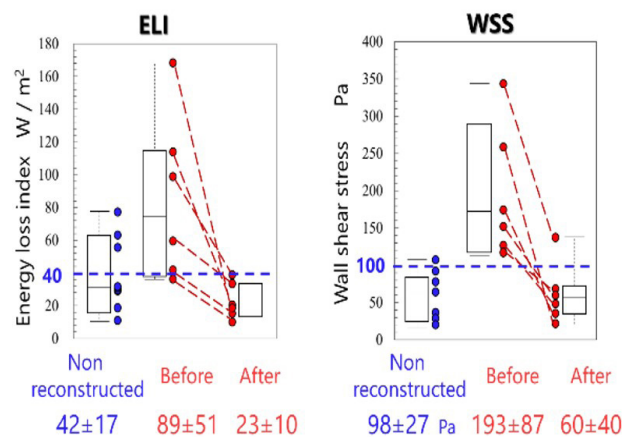


Figure 33: Pre- and postoperative changes in ELI and WSS

Figure 34 also shows how the streamlines and WSS distribution changed pre- and post-operatively, as well as the observed energy loss values. This clearly shows that even if the geometry appears to have a high cardiac load in the first stage of surgery, it can be improved by subsequent reconstruction.

Even when no stenosis or pressure gradient was observed on catheterization or echocardiography, the results suggest that CFD analysis can be used to determine surgical strategy and effectively reduce cardiac load.

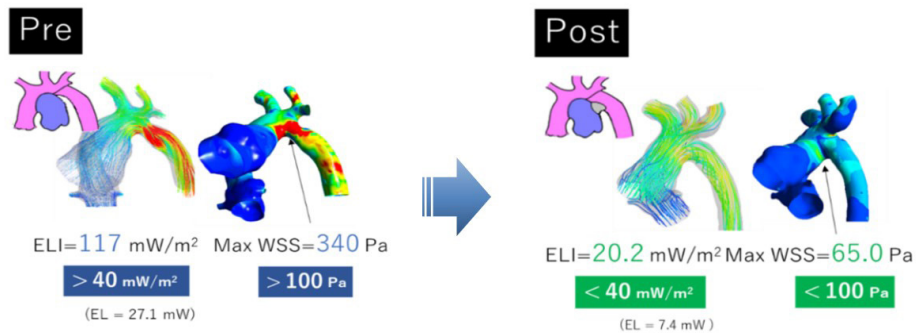


Figure 34: Pre- and post-operative changes in ELI and WSS as seen in the color map.

## 6. Evaluation of intracardiac vortical flow after mitral valve surgery with VFM (mechanical and biological valves) <sup>(23)</sup>

### Performance varies depending on the aspect of the vortex flow

This is a report showing that different methods of mitral valve surgery may affect the aspect of vortical flow in the left ventricle and the performance of the heart pump.

Visualization of intracardiac blood flow using ultrasound VFM showed counterclockwise vortical flow as shown in Figure 35 in a case after mechanical valve implantation in an anti-anatomical position and in a case after bioprosthetic valve replacement.

In the case of the post-bioprosthetic valve replacement, a large counterclockwise vortex was formed in the center of the ventricle, but the valve itself was soft and the vortex moved in a gliding manner. In addition, small vortices can be seen forming.

In three of the cases after mechanical valve implantation in the anti-anatomical position, asynchronous posterior wall motion was observed in early contraction, resulting in a reduced ejection fraction (EF).

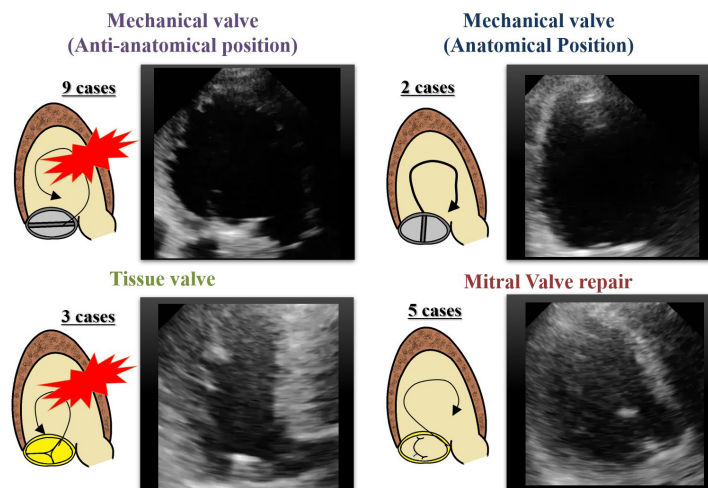


Figure 35 Intracardiac vortical flow after mechanical valve replacement (left) and biological valve replacement (right)

## How does the direction of the vortex change energy efficiency?

Figure 36 compares energy loss (EL) and dynamic pressure (KP) in systole and diastole in clockwise and counterclockwise vortices.

There was no significant difference in energy loss and dynamic pressure, but the EL/KP ratio, which indicates flow efficiency, was higher for the counterclockwise vortex, indicating lower efficiency.

On the other hand, during diastole, the clockwise vortex produced more energy and thus greater losses, and there was no significant difference in the EL/KP ratio.

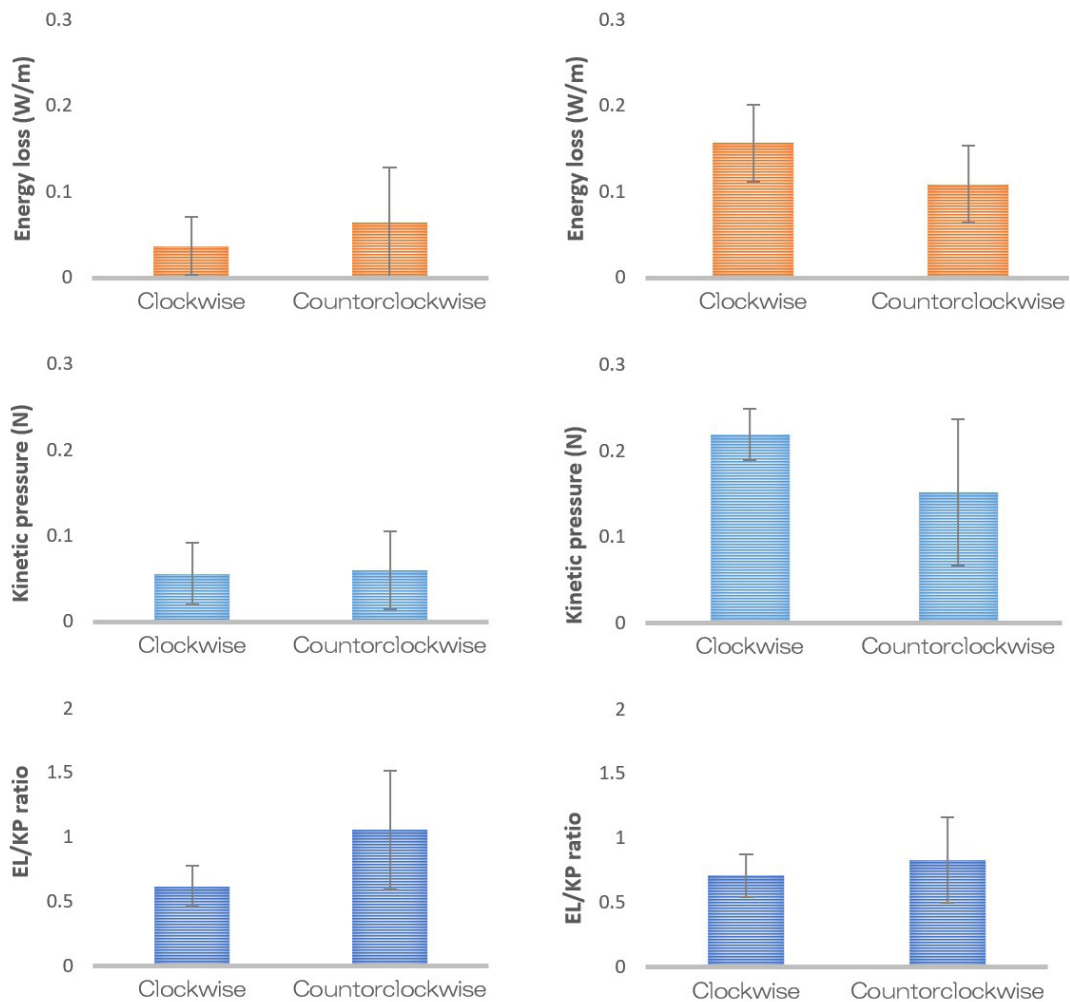


Figure 36 Energy loss (EL) and dynamic pressure (KP) during systole (left) and diastole (right), flow energy efficiency ratio (EL/KP). Differences occur depending on whether the vortex is clockwise or counterclockwise.

# Chapter 4: Various Indicators for Blood Flow Analysis

We have discussed three analysis methods (CFD, 4D Flow MRI, and ultrasound) and specific examples. Each of these methods can be used to calculate flow velocity vectors. Furthermore, the numerical values can be used to visualize various hydrodynamic indices.

This chapter will introduce those indicators.

## 1. Flow velocity vector is a basic indicator

### If you know the vectors, you know the whole process

The velocity vector is the most basic indicator of fluid dynamics. For example, when trying to understand the flow of a turbulent current in a river, if we know the "direction" and "magnitude" (i.e., vector) of the flow at a given location in the river, as shown in Figure 37, we can understand the overall flow.

All of the aforementioned analysis methods measure or calculate this flow velocity vector. Most of the hydrodynamic indices that will appear in the next section are indices that are calculated by using this flow velocity vector.

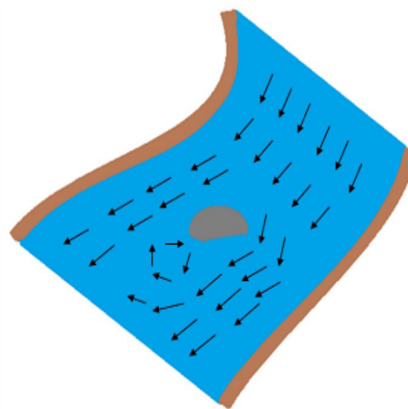


Figure 37: Vector simulating a flooding river and the direction of flow

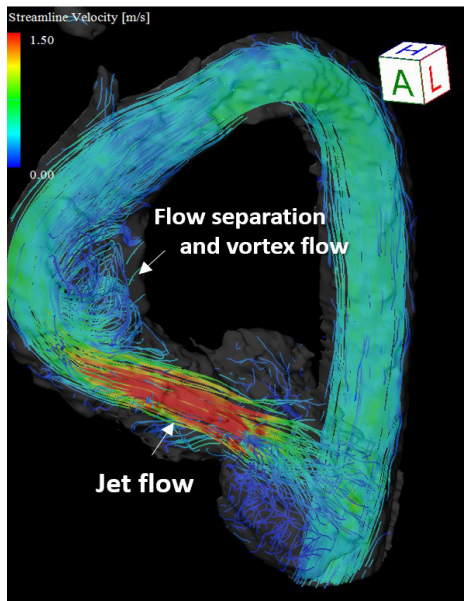
### Streamlines

#### How to visualize the flow (1)

There are two ways to view blood flow: streamlines, which connect the velocity vectors of particles at each coordinate when stopped at a certain time, and pathlines, which divide the fluid into numerous microparticles and track each of them in time.

A streamline is a smooth line drawn according to the direction of the blood flow velocity vector and can display the flow at a given instant in an easy-to-understand manner. By representing the flow as a line, the turbulence of the flow and the shape of the vortex can be confirmed.





As an example, consider the flow lines within the aorta, as shown in Figure 38. The direction of flow is drawn in a smooth line from the left ventricle to the aorta and then to the aortic arch. The blue areas represent areas of slow velocity and the red areas represent areas of high velocity.

In addition, spiraling streamlines can be seen. Visualization of streamlines can also confirm the presence of such eddy currents.

Figure 38: Streamlines in mild aortic valve stenosis.

Line represents flow direction and color represents flow speed (red is fast, blue is closer to zero speed).

## Pathlines

### How to visualize the flow (2)

A stream line is a line that represents the path of how a single particle in a fluid flows in a given period of time. Whereas a streamline represents "flow at a given moment," a stream trace line is used to show the route along which blood flows over time.

When used in cardiovascular applications, it shows where particles are located in systole and diastole during a single heartbeat. The difference is that streamlines can be visualized in moving images, while streamlines follow changes over time in images.

Figure 39 visualizes streamlines and flow trace lines side by side. Although the same technique is used to visualize the flow direction with lines, we can see that there is a slight difference between the movement of particles and the flow direction.

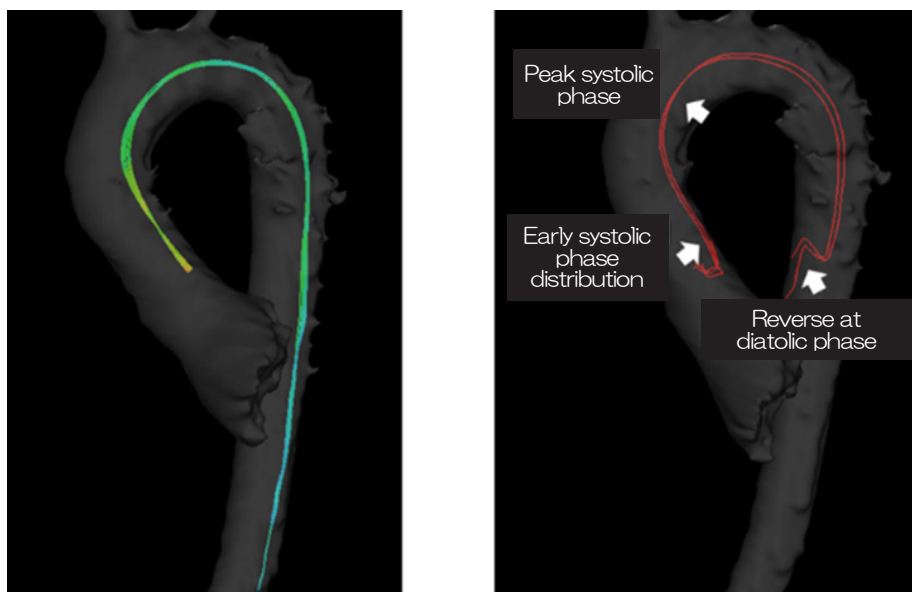


Figure 39 Streamlines (left) and streamlines (right) of intra-aortic blood flow.

The streamlines show where the particles are located within the heartbeat.

## 2. Energy loss (EL)

### Energy Loss

#### What causes the heart to lose pulsating energy?

The beating of the heart is responsible for delivering energy to the periphery. Therefore, if extra energy is lost somewhere, the burden on the heart increases. An indicator of how much energy is lost within a target area is Energy Loss (EL).

Energy is lost mainly through conversion into heat and sound. The conversion is attributed to "friction at the wall" and "turbulence in the flow."

"Friction at the wall" is a value that increases with higher blood viscosity or flow velocity. Therefore, in the geometry shown in Figure 40, the flow is as fast as a jet at the site of stenosis, and thus more energy is lost due to wall friction.

Also, the flow is "disrupted" posterior to the stenosis site due to rapid dilation. This is another factor contributing to the high energy loss.

Basically, "total pressure" is used to calculate these energy losses.

Total pressure is the sum of "static pressure" and "kinetic pressure" and is said to represent the potential energy of the flow. Therefore, energy loss can be defined by taking the difference between the total pressure at the defined inlet and the total pressure at the outlet.

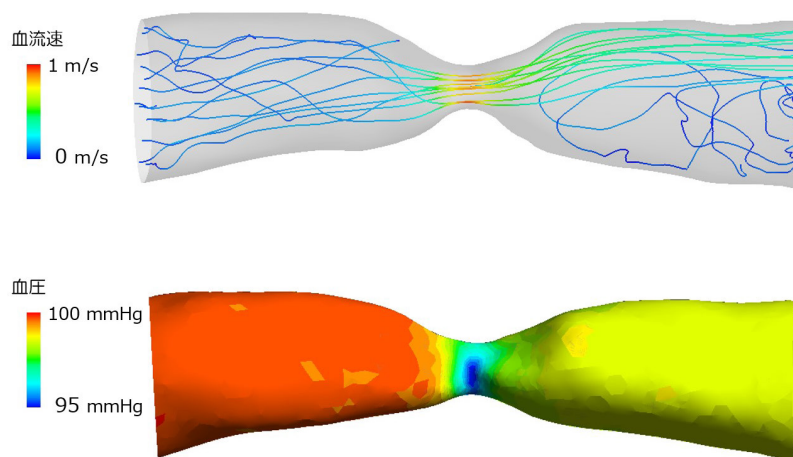


Figure 40: Flow velocity (top) and static pressure distribution (bottom) at the site of stenosis

#### Pressure information is essential for EL calculations

Energy loss (EL) can be calculated as the difference in total pressure. In other words, to calculate energy loss, pressure information is needed; CFD gives pressure (strictly relative pressure values), but actual measurement would require invasive catheter measurements. However, methods have been developed that can be calculated from the flow velocity by the aforementioned "observation".

It utilizes the fluid dynamics equation called viscous dissipation, also known as "viscous dissipative energy loss" or "viscous frictional energy loss."

Figure 41 shows the velocity distribution and the energy loss calculated from it. It can be seen that large energy losses occur where the flows collide and where the flows peel off and rub against each other.

By integrating the loss values all within this region, the overall energy loss can be quantified. It has been mathematically proven that this overall integrated energy loss is consistent with the energy loss based on total pressure <sup>(24)</sup>.

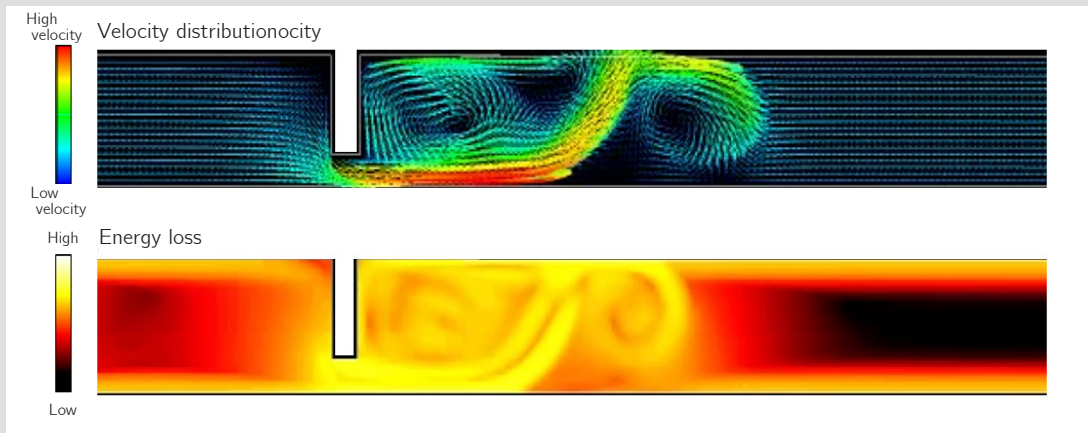


Figure 41: Flow field and viscous frictional energy loss at an area of constriction

To obtain the viscous dissipative energy loss, the flow velocity distribution is required, which turns out to be an excellent indicator that can be calculated not only by CFD, but also by velocimetry devices such as MRI and ultrasound. In addition, it can be calculated from the flow velocity in each micro-region, allowing the spatial distribution to be visualized.

Figure 42 visualizes the velocity distribution obtained from MRI (left) and the viscous dissipative energy loss calculated from it (right).

#### Streamline (Streamlines )

The direction and velocity of blood flow can be checked. This allows for the identification of abnormal accelerated blood flow and the shape of vortexes.

#### Energy loss

Flow Energy Loss, which quantifies cardiac load, can be calculated and visualized in white intensity.

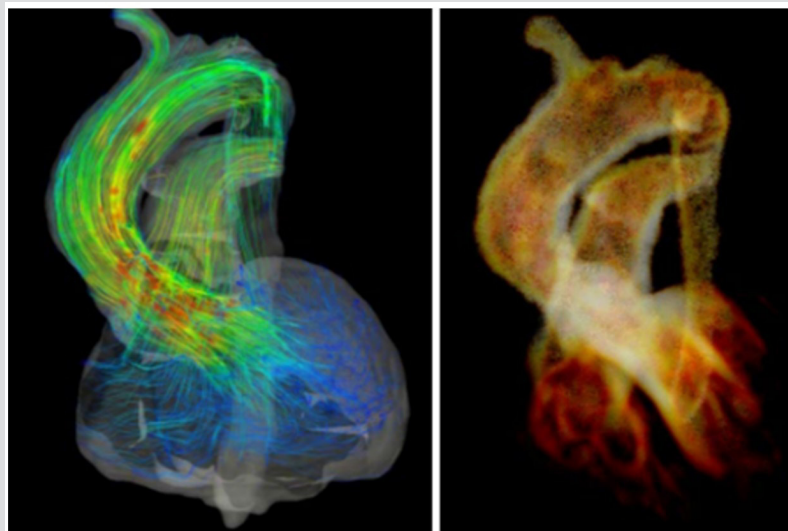


Figure 42 Streamlines from heart to aorta (left) and distribution of energy loss (right)

### 3. Wall shear stress (WSS)

#### Wall shear stress WSS

#### WSS can detect atherosclerosis and aneurysms

Stress is used to describe the force generated inside an object. In blood vessels, that object is the vessel wall. Knowing the stresses in the vascular wall is important for understanding the causes of vascular endothelial damage.

Stresses generally take the form of a tensor, and although it is not possible to write them down in a general way, such as "this is the magnitude," they can be described by two components, "vertical stress" and "shear stress," as shown in Figure 43.

Vertical stress is the magnitude of stress in the direction normal (perpendicular) to the plane of the object, while shear stress is the stress acting in other directions.

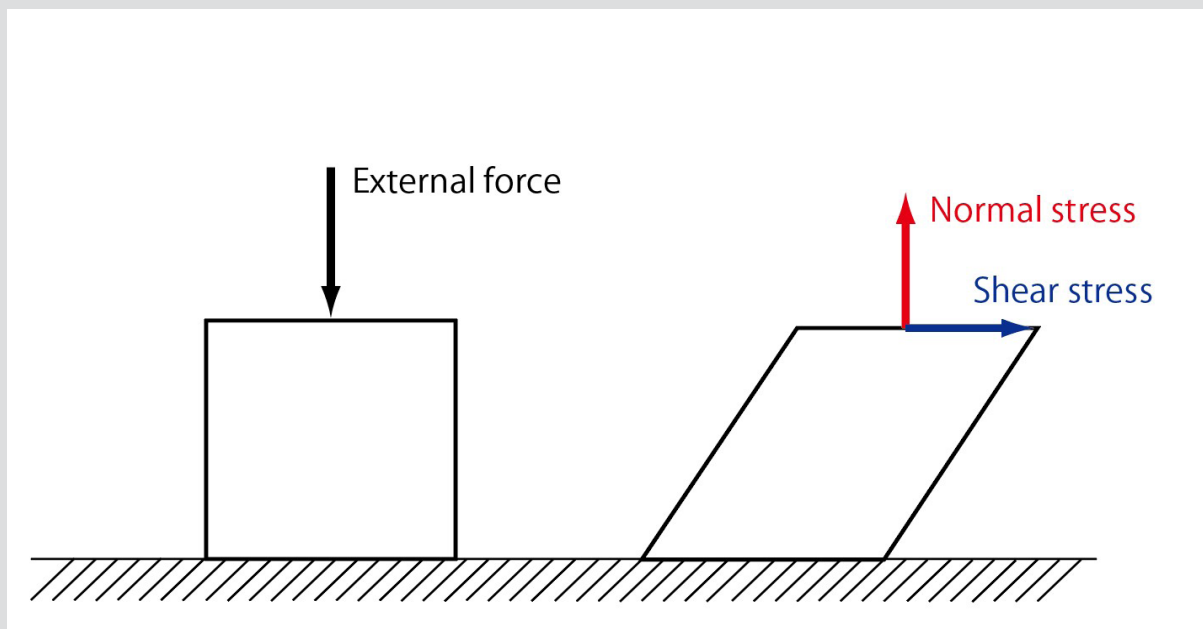


Figure 43 Vertical and shear stresses in an object

In blood flow analysis, the equivalent of a vertical external force is the force of blood pushing against the vessel wall, or blood pressure. The stress caused by this can be calculated by structural analysis using solid mechanics. Shear stress, on the other hand, can be calculated from fluid mechanics alone, assuming a rigid wall surface (i.e., a solid, non-deforming wall such as glass).

The stress calculated from fluid mechanics is called "wall shear stress (WSS)," which is an indicator frequently used in blood flow analysis studies because it is thought to be caused by the development and progression of atherosclerosis and the growth of aneurysms <sup>(25) (26)</sup>.

WSS is an indicator that can calculate "the value at a certain place at a certain moment" due to its calculation method. Therefore, it is possible to calculate its temporal average (TAWSS: time-averaged WSS), temporal variation (TWSSG: temporal WSS gradient), and spatial variation (SWSSG: spatial WSS gradient).

## To obtain a reliable WSS value

The viscosity of the blood and the velocity gradient around the wall are needed to calculate WSS.

Figure 44 illustrates the direction of calculation of a simplified velocity gradient. Since the velocity at the wall surface is zero, the important value that determines the gradient is the velocity at the point closest to the wall surface.

The flow velocity profile has a nonlinear shape, as shown in Figure 44 left, with a gradually loosening gradient. Therefore, if the point at which the gradient is calculated is far away, the value will differ significantly from the theoretical velocity gradient, and if a close point is obtained, a reliable value can be calculated.

With CFD, the distance from the wall surface can be set in detail, allowing reliable WSS values to be calculated. On the other hand, in the case of actual measurement modalities (MRI and ultrasound), the distance from the wall surface cannot be determined because the resolution is fixed. Therefore, in the visualization of MRI and ultrasound measurements, interpolation and other devices must be used to calculate them, which is why "WSS can calculate reasonable values in CFD."

However, this is not to say that the WSS that can be obtained with MRI is unreliable; it is an index that can be adequately discussed with respect to spatial relative values.

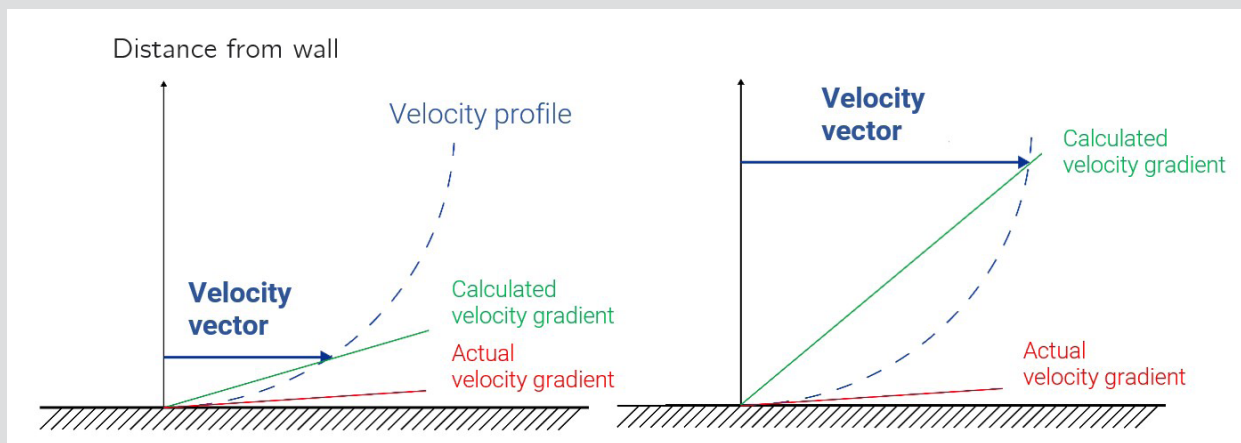


Figure 44: Change in velocity gradient at different sample points from the wall (simplified velocity gradient calculation)

## Oscillatory shear index

### OSI to quantify fluctuations in time variation

OSI (oscillatory shear index) is the degree to which the direction of WSS changes over time (within one beat in blood flow analysis) and quantifies the "fluctuation" of WSS over time.

OSI is an index that takes values between 0 and 0.5. The closer to 0.5, the higher the variation of WSS within one heartbeat, and the closer to 0, the more WSS is always in one direction.

It has been reported that where OSI is high, endothelial cells produce reactive oxygen species, which may influence the progression of vascular endothelial lesions.



Figure 45 shows an example of when OSI is high. Normally in blood vessels, the flow is progressive in systole and retrograde in diastole. If there is an obstacle such as the plaque in the figure, a vortex is created. This prevents the flow from being in a constant direction, resulting in a high OSI.

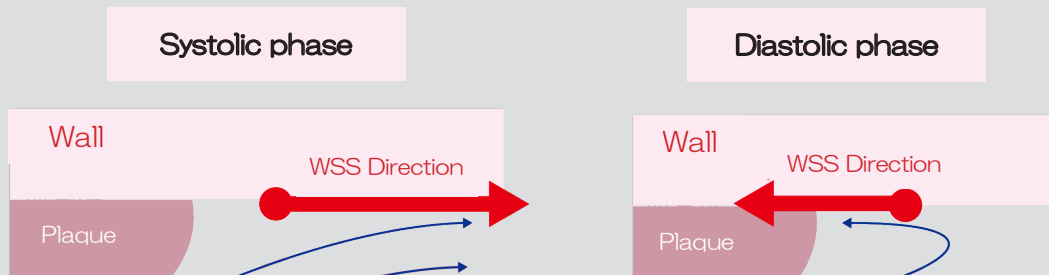


Figure 45: Example of a high OSI. Progressive flow in systole but retrograde blood flow appears in diastole. The presence of obstructions such as plaques cause the fluctuation of the WSS, resulting in a higher OSI.

## 4. Three indicators for vortex

### Purposeful eddies and disorganized, harmful eddies exist

There are vortices that exist in vivo with a purposeful effect: to smoothly turn the direction of flow in the normal left ventricle, to close valves that form in the sinus of Valsalva, and to direct blood flow to the coronary arteries.

On the other hand, there are also eddy currents that are not captured effectively, called turbulence. Turbulence is a swirling eddy, called a vortex, that occurs in disorder at various scales .

The aspect of vortical flow is a major factor in characterizing hemodynamics.

In the following, we will discuss mathematical indicators that quantify the vortex.

### Vorticity

#### Vortex index (1)

Vorticity, a measure that quantifies the presence and strength of swirling velocity vectors, has long been used in meteorology to provide insight into the big-picture weather conditions.

Indicates how the flow is turning with respect to the direction of flow at a given point.

The magnitude of the vorticity is zero in the upper part of Figure 46.

On the other hand, a non-zero vorticity is a state in which a spatial distribution exists in the flow velocity, causing the object to swirl, as shown in the lower part of Figure 46. Therefore, a non-zero vorticity indicates the presence of a vortex, and its magnitude is a measure of the strength of the swirl.

In 3D, vorticity is calculated as a vector, but a visual understanding of what phenomenon it represents is difficult.

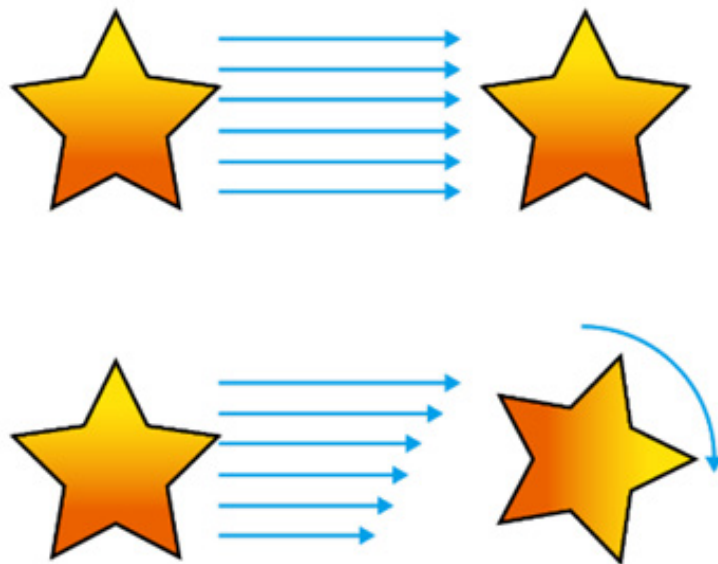


Figure 46: Stars flowing straight (top) and rotating (bottom)

## Cycle

### Vortex index (2)

Circulation is an indicator of vorticity strength.

Since circulation is an index expressed in terms of the area of the vorticity vector, the larger the vorticity vector, the larger the circulation, and the larger the area to be integrated (the closed curve that determines the vortex), the larger the circulation. In other words, it is an indicator of the strength of the vortex itself or the size of the vortex.

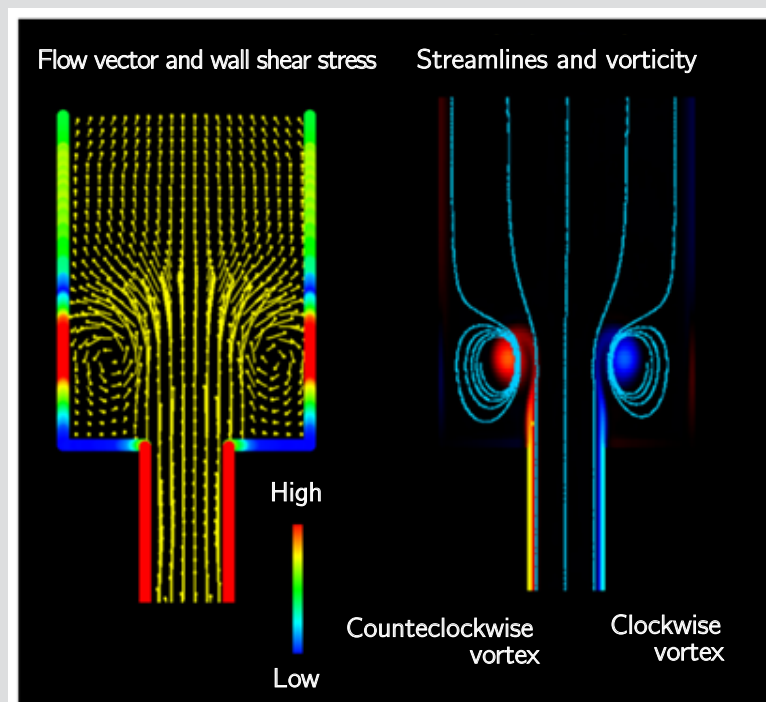


Figure 47 Velocity vector and wall shear stress (left), streamlines and vorticity (right) in 2-D flow field

## Helicity

### Vortex index (3)

Helicity is a measure that evaluates helical flow. By definition, it uses vorticity and velocity and integrates over all regions.

Helicity is low for a clean spiral flow and high for a turbulent flow.

However, even a relatively clean helical flow will have a high Helicity value if the velocity of the flow is high enough. Therefore, it is easy to get relatively high values during systole, but that does not necessarily mean that it is a problematic helical flow. It is necessary to evaluate the flow field by observing what kind of flow field is present.

If the rotation is clockwise relative to the flow direction, it takes a positive value; if counterclockwise, it takes a negative value. This is a difficult indicator to use in situations such as pulsation, where the flow direction changes instantaneously, but when limited to systole, the flow direction is easy to understand and visualization in Helicity becomes easier to understand.

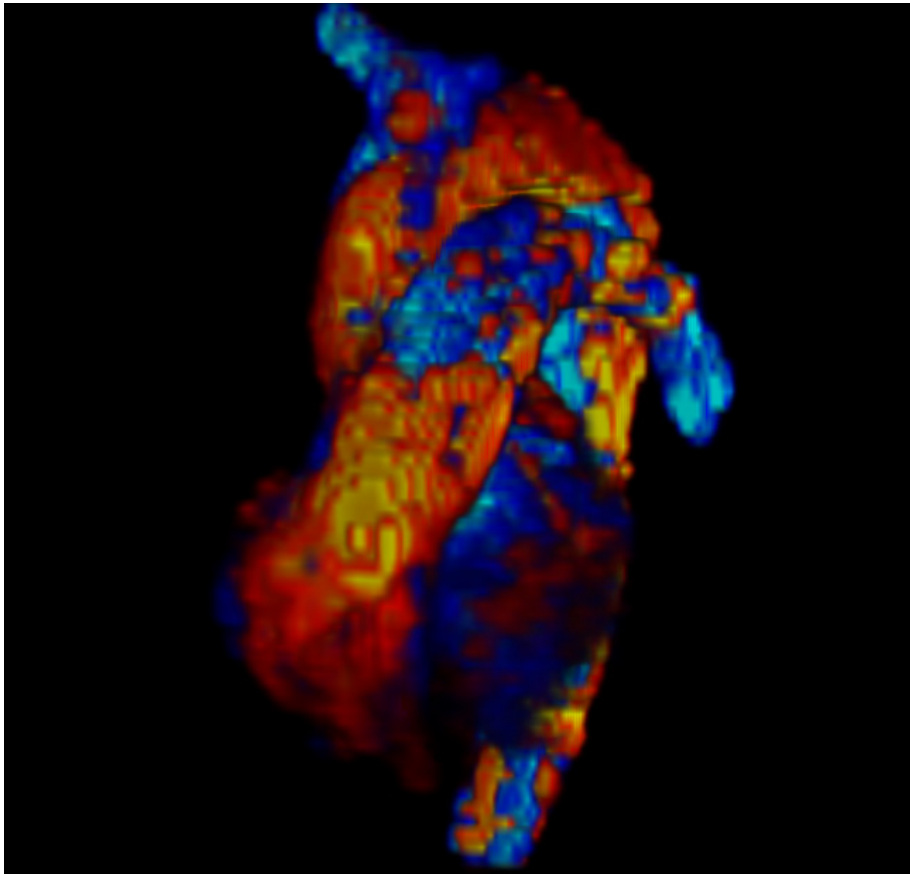


Figure 48 Visualization of Helicity with 4D FLOW MRI

Blood flow in the aorta is efficiently transported by helical flow.

Helicity is a measure of the strength of that helix.

# Appendix 1: Fluid Dynamics in Equations

In this chapter, we will describe not only the mathematical expressions of the indicators that have appeared so far, but also the mathematical formulas used in fluid dynamics. Under what definitions the visualization images so far are created will be explained with mathematical expressions. This is a mathematical and very difficult chapter, so it is written for those who like and want to understand mathematics. Each indicator is also described in "Various Indicators Useful for Blood Flow Analysis (p. 38)," so it is recommended that you refer mainly to that section.

## Governing equation

A governing equation is an equation that describes a phenomenon in general, not just a fluid. Here, we describe the governing equations for incompressible fluids, such as blood. Incompressible fluid is a term that refers to a fluid with a constant density, and our familiar fluid phenomena (air circulation in a room, flow in water, etc.) belong to this category. On the other hand, compressible fluid refers to special situations such as the gas in the piston of a car engine or a fluid with a velocity exceeding Mach speed. The governing equations for incompressible fluids, the subject of this study, are the Navier-Stokes equation and the continuity equation.

The incompressible Navier-Stokes equation can be shown with time  $t$  as follows

$$\rho \left( \frac{\partial u_i}{\partial t} + \frac{\partial(u_i u_j)}{\partial x_j} \right) = -\frac{\partial p}{\partial x_i} + \mu \frac{\partial}{\partial x_j} \left( \frac{\partial u_i}{\partial x_j} + \frac{\partial u_j}{\partial x_i} \right)$$

Where  $\rho$  is the density,  $u_i$  is the flow velocity,  $\frac{\partial}{\partial x_i}$  is the spatial differential operator (meaning gradient),  $\frac{\partial(u_i u_j)}{\partial x_j}$  is the inertia term,  $\frac{\partial p}{\partial x_i}$  is the pressure gradient, and  $\mu \frac{\partial}{\partial x_j} \left( \frac{\partial u_i}{\partial x_j} + \frac{\partial u_j}{\partial x_i} \right)$  is the viscosity term. The notation " $u_i$ " is an extension of the mathematical notation for vectors called tensors. For an incompressible fluid with constant density, the above notation is used because the density  $\rho$  can be taken from the first time derivative term. To this we add the expression for continuity, which implies conservation of mass.

$$\frac{\partial u_i}{\partial x_i} = 0$$

This equation of continuity can be summarized in a form that describes only the divergence of the fluid, with the density being constant and unaffected by either time or space variations. Also, since it is a vector, it has a component  $\left( \frac{\partial}{\partial x}, \frac{\partial}{\partial y}, \frac{\partial}{\partial z} \right)$  in the three-dimensional case. Thus, the above equation can be rewritten as in the equation below.

$$\frac{\partial u_i}{\partial x_i} = \frac{\partial u_1}{\partial x_1} + \frac{\partial u_2}{\partial x_2} + \frac{\partial u_3}{\partial x_3} = \frac{\partial u_x}{\partial x} + \frac{\partial u_y}{\partial y} + \frac{\partial u_z}{\partial z}$$

Here we review the relationship between vectors and scalars. The inner product of vectors is a scalar, which means that the velocity components in each direction are differentiated in each of those directions and added together. Zero velocity divergence means that the fluid does not suddenly disappear or gush out. In the above equation,  $\frac{\partial u_i}{\partial x_i}$  is the divergence of velocity. And assuming a Newtonian fluid with constant viscosity like blood, the Navier-Stokes equations can be simplified as follows

$$\rho \left( \frac{\partial \mathbf{u}}{\partial t} + \mathbf{u} \cdot \nabla \mathbf{u} \right) = -\nabla p + \mu \Delta \mathbf{u}$$

Here  $p$  is the pressure,  $\mu$  is the viscosity coefficient, and  $\Delta$  is the Laplacian, expressed as  $\nabla \cdot \nabla$  or  $\nabla^2$ . This is the governing equation describing the fluid, and CFD finds the flow velocity and pressure to satisfy it.

## boundary condition

Simply determining the domain in which the fluid flows and applying the governing equations is not enough to do the calculation. The solution is not possible without knowing how much energy will flow in from outside the domain. Therefore, boundary conditions such as velocity or surface force are set at the boundaries of the space. The boundary condition that gives the velocity is called the fundamental boundary condition or Dirichlet boundary condition, and the boundary condition that gives the surface force is called the natural boundary condition or Neumann boundary condition. Since the unknown in the governing equations above is the flow velocity, which is in vector form, the boundary conditions must also be in vector form.

## Dirichlet boundary condition

This section describes the boundary conditions used in blood flow analysis. For the Dirichlet boundary condition, let  $u_\Gamma$  be the flow velocity at the boundary  $\Gamma$ , and set.

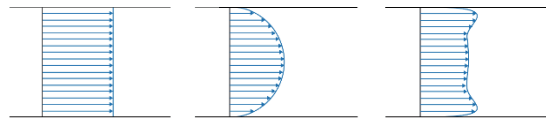
$$u_\Gamma = \mathbf{v}$$

The condition is such that the flow velocity  $\mathbf{v}$  is applied directly to the unknowns. For example, if we want to give the flow rate as a boundary condition, we need to transform the flow so that the velocity is given at all points in the inflow section. For this conversion, a flow profile must be specified. The profile is an expression in the form of a velocity vector passing through a plane defined in the flow field, as shown in the example flow velocity profile in the figure below.

The easiest is the uniform flow on the left, but the magnitude of the velocity should be zero at the wall surface, so the profile is not possible as a phenomenon.

The center is called the Hagen-Poiseuille flow, which is known to develop into such a flow when a steady flow is sufficiently developed. When the flow becomes a pulsating flow, it takes the shape shown on the right. There are minor changes depending on the beating conditions, which are known to vary with a value called the Womersley number. In the case of blood, just because it is beating does not necessarily mean that it takes the shape shown on the right. In actual analysis, to simulate a developed flow, the inflow is often extended and adjusted to flow uniformly so that the developed flow enters the area of interest.

Dirichlet boundary conditions are essential in solving the equation because they determine the values, but if they are set at all boundaries, the calculation will not work well. This is because it is difficult to satisfy both conservation laws and boundary conditions without an escape route (Neumann boundary condition) somewhere.



## Neumann boundary condition

Neumann boundary conditions are boundary conditions that determine the gradient of a value, unlike Dirichlet boundary conditions, which directly specify unknowns. For example, if the difference between 100 and 80 is 20, and the difference between 40 and 20 in the same interval is also 20, then both have the same slope. Thus, the slope setting is more lenient than the absolute value setting. However, if such a setting is used for the inflow boundary condition, it is difficult to satisfy the conservation law because it is not known how much energy will flow into the region of interest, and there is no guarantee that it will diverge easily or emerge as a solution. It follows that setting the boundary conditions at the appropriate locations requires experience and computational engineering knowledge. The formulation is as follows

$$\boldsymbol{\sigma} \cdot \mathbf{n} = \mathbf{h}$$

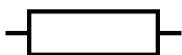
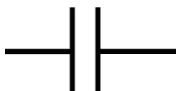

$\mathbf{h}$  is the surface force and  $\mathbf{n}$  is the unit normal vector at the boundary. In blood flow analysis it is often transformed as follows

$$\boldsymbol{\sigma} \cdot \mathbf{n} = p\mathbf{n}$$

This  $p$  can be incorporated as a boundary condition or as  $\nabla p$  in the pressure range.

## Boundary condition implementation: Lumped Parameter Model

As mentioned above, flow and pressure are used as boundary conditions. However, in actual living organisms, flow and pressure are regulated by a complex interplay of various factors, and determining the conditions requires some ingenuity. For example, when analyzing the aortic arch, its blood flow exchanges energy with the heart and peripheral vessels and vasculopathy, and their behavior must also be calculated. Since we only want to know the flow in the aortic arch, we want to omit the calculations for the other organs as much as possible. A lumped parameter model is a simple way to simulate closed circuits in the circulatory system by modeling everything except the domain to be calculated as a very simple electrical circuit. The current is considered as blood flow and the voltage as blood pressure, and the whole body circulatory system is modeled by replacing each part with electrical components such as resistors, capacitors, coils, and so on. In numerical fluid analysis, calculations are performed in three dimensions, but the lumped parameter model is a zero-dimensional model. To combine the two, the flow rate is input into the lumped parameter model, the pressure is determined, and used as a boundary condition for each iteration of the calculation

<p>Resistor:</p> 	<p>Vascular resistance</p> <p>the higher the blood flow, the higher the pressure</p>
<p>Capacitors:</p> 	<p>Compliance:</p> <p>vascular capacitance increases when blood pressure rises and decreases when it falls</p>
<p>Coil:</p> 	<p>Inertial force</p> <p>keeps the flow rate even when blood pressure changes</p>



## Fluid Indicators

### Reynolds number

When you begin to study fluid mechanics, Reynolds number comes up at the beginning. The Reynolds number **Re** is a dimensionless number that describes the properties of a fluid. If the representative velocity of the flow is **U**, the representative length is **L**, and the kinematic viscosity is **v**, it is defined as follows

$$\text{Re} = \frac{UL}{\nu} = \frac{\rho UL}{\mu}$$

As mentioned above, **ρ** and **μ** are the density and viscosity coefficients. As the Reynolds number increases, the Navier-Stokes equation becomes a turbulent solution. Generally speaking, a small Reynolds number indicates laminar flow, 2,300-4,000 is the transition zone where both laminar and turbulent flow can occur, and above that, the flow is turbulent.

For intra-tube flow, such as blood flow, the representative length is the vessel diameter. For reference, let us calculate the Reynolds number for flow in the aorta. Assuming a mean flow velocity of 1.0 m/s, a vessel diameter of 20 mm, a blood density of 1,060 kg/m<sup>3</sup>, and a viscosity coefficient of 0.004 Pa-s, the value is 5,300. Since there is a wide range of values, such as flow velocity during systole and diastole and vessel diameter of about 15 mm to 25 mm, the Reynolds number of intra-aortic blood flow is generally said to be about 1,000~10,000. Therefore, it is not possible to say that the blood flow is turbulent in general.

Often experiments are scaled to this Reynolds number, since the same Reynolds number can be said to have the same hydrodynamic properties. For example, a large aircraft experiment requires a certain amount of equipment, but a small experimental facility can produce similar results if the experiments are performed with the same Reynolds number.

### Streamline

In "Various Indicators for Blood Flow Analysis (p.35)," we focused on what a streamline is and how it can be visualized. In this section, we explain the mathematical definition. Let us define a streamline as a position that varies with the parameter **s** from a start point to an end point. Then it can be written as **x<sub>s</sub>(s)**. This is a vector of functional type meaning that the position **x<sub>s</sub>** changes as **s** changes. The subscript **s** stands for streamline. At the starting point it can be written as **x<sub>s</sub>(0)**.

The tangent vector of this streamline can be obtained by differentiating the position vector by the parameter **s** and can be written as **dx<sub>s</sub>(s)/ds**. Then the relationship between the velocity **u(x<sub>s</sub>(s))** at position **x<sub>s</sub>(s)** and its tangent can be written as

$$\frac{dx_s(s)}{ds} \times u(x_s(s)) = \mathbf{0}$$

Here **x** represents the outer product of the vectors, which is a zero vector, meaning that the two vectors (the stream tangent and the velocity vector) point in the same direction. In other words, this equation shows that the velocity vectors are connected to form the streamline itself.

#### About Position Vector

Position vector, and as a matter of course we write position as a vector, but if you are not familiar with it, you may think of point **P** when you think of position. It may seem that a point is not a vector, but position also has three components, **x**, **y**, and **z**, and can be regarded as a vector from the origin.

Also, in the field of continuum mechanics, the bolded **x** generally denotes the position vector. In this booklet, the position vector of a streamline is placed as **x<sub>s</sub>**, and is distinguished from other position vectors by this subscript **s**.

### Flowline

We mentioned earlier that a pathline is a line that represents how a single particle flows. The trace line can also be regarded as a position vector **x<sub>p</sub>(t)** that varies with time **t**, where **P** stands for pathlines. The tangent vector of the pathlines can be obtained by differentiating the position vector by the parameter **t**, and can be written as **dx<sub>p</sub>(t)/dt**. From this tangent vector, the following relationship can be written.

$$\frac{dx_p(t)}{dt} = u(x_p(t), t)$$

This means that the tangent vector of the trace line and the velocity of the flow at that location are the same, indicating that the particles are moving in the fluid.

## Energy loss

Energy loss  $EL$  can be expressed by the following equation.

$$EL = (P_{\text{total}})_{\text{in}} Q_{\text{in}} - (P_{\text{total}})_{\text{out}} Q_{\text{out}}$$

Here,  $Q_{\text{in}}=Q_{\text{out}}$  because the flow rate is conserved, but the above equation is derived from the calculation results as follows

$$EL = \int_{\Gamma} \left( \frac{1}{2} \rho \mathbf{u}^2 + P \right) (\mathbf{u} \cdot \mathbf{n}) d\Gamma_{\text{in}} - \int_{\Gamma} \left( \frac{1}{2} \rho \mathbf{u}^2 + P \right) (\mathbf{u} \cdot \mathbf{n}) d\Gamma_{\text{out}}$$

Each term represents the inlet and outlet energies, expressed in integral form at the inlet surface  $\Gamma_{\text{in}}$  and the outlet surface  $\Gamma_{\text{out}}$ . (The boundary surface  $\Gamma$  is a convenient notation for boundaries regardless of dimension. In the two-dimensional case it is the line integral, and in the three-dimensional case it is the area integral.) As mentioned earlier, the energy loss is derived as the difference between the total pressure at the inlet surface  $\Gamma_{\text{in}}$  and the outlet surface  $\Gamma_{\text{out}}$  multiplied by the flow rate, where  $\rho \mathbf{u}^2 / 2$  represents the dynamic pressure and  $P$  represents the static pressure, which add up to the total pressure. Also,  $\mathbf{n}$  represents the unit normal vector at the surface, so  $\mathbf{u} \cdot \mathbf{n}$  is the flow velocity toward the surface. Integrating this at that surface gives the flow rate.

### About Units

Let us now consider the units of the above equation. It is important to look at the units in order to consider whether the equation is correct and what this value means. First, density  $\rho$  is in  $\text{kg}/\text{m}^3$ , velocity  $\mathbf{u}$  is in  $\text{m}/\text{s}$ , and static pressure  $P$  is in  $\text{Pa}$ , but to keep the unit system consistent, we will use  $\text{kg}/(\text{m} \cdot \text{s}^2)$ . Since the normal  $\mathbf{n}$  has no units,  $\mathbf{u} \cdot \mathbf{n}$  is  $\text{m}/\text{s}$ . Finally,  $d\Gamma$  is  $\text{m}^2$  since it is a minute area.

$$\left( \frac{\text{kg} \cdot \text{m}^2}{\text{m}^3 \cdot \text{s}^2} + \frac{\text{kg}}{\text{m} \cdot \text{s}^2} \right) \frac{\text{m}}{\text{s}} \cdot \text{m}^2 = \frac{\text{kg} \cdot \text{m}^2}{\text{s}^3} = W = J/\text{s}$$

Now let's calculate the units of energy loss based on this.

Thus, we were able to calculate the units of energy loss. If the units are not correct, the addition is not valid, so the parentheses in which the total pressure is calculated are also a valid equation. In this way, we can deepen our understanding while converting units.

Now, the energy loss determined from the flow velocity is also shown below.

$$EL = \int_{\Omega} \frac{1}{2} \mu \sum \left( \frac{\partial u_i}{\partial x_j} + \frac{\partial u_j}{\partial x_i} \right)^2 d\Omega$$

All that is needed in this calculation is the viscosity coefficient  $\mu$ , the gradient of the flow velocity  $\mathbf{u}$ , and the area  $\Omega$  (area  $\Omega$  is a convenient notation for an area, regardless of dimension. In the case of two dimensions, it is the area integral, and in the case of three dimensions, it is the volume integral) to obtain the energy loss. In understanding this equation, we need to know something new called index notation. In the first equation, we wrote it in terms of  $i$  and  $j$ . These numbers are called indices. In the case of three dimensions,  $i, j = 1, 2, 3$ , and so on, repeating from 1 to 3, respectively. The following is an example of three dimensions.

$$EL = \int_{\Omega} \frac{1}{2} \mu \sum \begin{pmatrix} \left( \frac{\partial u_1}{\partial x_1} + \frac{\partial u_1}{\partial x_1} \right)^2 & \left( \frac{\partial u_1}{\partial x_2} + \frac{\partial u_2}{\partial x_1} \right)^2 & \left( \frac{\partial u_1}{\partial x_3} + \frac{\partial u_3}{\partial x_1} \right)^2 \\ \left( \frac{\partial u_2}{\partial x_1} + \frac{\partial u_1}{\partial x_2} \right)^2 & \left( \frac{\partial u_2}{\partial x_2} + \frac{\partial u_2}{\partial x_2} \right)^2 & \left( \frac{\partial u_2}{\partial x_3} + \frac{\partial u_3}{\partial x_2} \right)^2 \\ \left( \frac{\partial u_3}{\partial x_1} + \frac{\partial u_1}{\partial x_3} \right)^2 & \left( \frac{\partial u_3}{\partial x_2} + \frac{\partial u_2}{\partial x_3} \right)^2 & \left( \frac{\partial u_3}{\partial x_3} + \frac{\partial u_3}{\partial x_3} \right)^2 \end{pmatrix} d\Omega$$

Thus, we see that it was actually a matrix notation. So what do the subscript numbers mean? First, the flow velocity can be expressed in component notation as  $\mathbf{u} = (u_x \ u_y \ u_z)$ , where  $u_x$  is the x-directional component of the velocity,  $u_y$  is the y-directional component, and  $u_z$  is the z-directional component. The position vector can also be expressed in component notation as  $\mathbf{x} = (x \ y \ z)$ . Thus, the first component of  $\mathbf{u}$  is  $u_x$ , the second component of  $\mathbf{x}$  is  $y$ , and so on. Thus, the previous equation can be rewritten as follows

$$EL = \int_{\Omega} \frac{1}{2} \mu \sum \begin{pmatrix} \left( 2 \frac{\partial u_x}{\partial x} \right)^2 & \left( \frac{\partial u_x}{\partial y} + \frac{\partial u_y}{\partial x} \right)^2 & \left( \frac{\partial u_x}{\partial z} + \frac{\partial u_z}{\partial x} \right)^2 \\ \left( \frac{\partial u_y}{\partial x} + \frac{\partial u_x}{\partial y} \right)^2 & \left( 2 \frac{\partial u_y}{\partial y} \right)^2 & \left( \frac{\partial u_y}{\partial z} + \frac{\partial u_z}{\partial y} \right)^2 \\ \left( \frac{\partial u_z}{\partial x} + \frac{\partial u_x}{\partial z} \right)^2 & \left( \frac{\partial u_z}{\partial y} + \frac{\partial u_y}{\partial z} \right)^2 & \left( 2 \frac{\partial u_z}{\partial z} \right)^2 \end{pmatrix} d\Omega$$

Once written down to this point, it is now easier to understand the calculation by hand. The calculation is completed by adding up all the matrix elements according to  $\Sigma$  and then integrating in the domain. The advantage of index notation is that it not only shortens the notation, but also accommodates differences in dimension. This means that the notation is easy to generalize. Also, in programming, operations using indexes are by far easier to describe. Having different notations for hand calculations and on the computer may seem confusing at first glance, but each notation has its own convenience. Now, finally, a two-dimensional version of the above equation is also shown.

$$EL = \int_{\Omega} \frac{1}{2} \mu \sum \begin{pmatrix} \left(2 \frac{\partial u_x}{\partial x}\right)^2 & \left(\frac{\partial u_x}{\partial y} + \frac{\partial u_y}{\partial x}\right)^2 \\ \left(\frac{\partial u_y}{\partial x} + \frac{\partial u_x}{\partial y}\right)^2 & \left(2 \frac{\partial u_y}{\partial y}\right)^2 \end{pmatrix} d\Omega$$

## Wall Shear Stress

The WSS vector  $\boldsymbol{\tau}$  can be calculated by using the velocity gradient around the wall.

$$\boldsymbol{\tau} = \mu \frac{\partial(\mathbf{u} - (\mathbf{u} \cdot \mathbf{n}_y)\mathbf{n}_y)}{\partial y}$$

where  $y$  is the coordinate system perpendicular to the wall and  $\mathbf{n}_y$  is the normal to the wall in the  $y$  direction. The differential term is subtracted from the vertical component to extract the velocity component horizontal to the wall. Thus, it represents the gradient of the flow velocity along the wall, which indicates how much higher the velocity along the wall becomes as you move away from the wall. This is multiplied by the viscosity factor to compute the WSS vector; if you want the WSS to be a scalar quantity, take the norm of the WSS vector.

$$WSS = \|\boldsymbol{\tau}\|$$

The norm is an operator that takes the magnitude of a vector.

## OSI

OSI is an equation related to time because it represents the fluctuation of WSS.

$$OSI = \frac{1}{2} \left(1 - \frac{\boldsymbol{\tau}^{NM}}{\boldsymbol{\tau}^{MN}}\right)$$

where the subscripts  $\boldsymbol{\tau}^{NM}$  and  $\boldsymbol{\tau}^{MN}$  mean the norm of the mean (norm of the mean) and the mean of the norm (mean of the norm), respectively. The definitions are given below.

$$\boldsymbol{\tau}^{NM} = \frac{1}{T} \left\| \int_0^T \boldsymbol{\tau} dt \right\|$$

$$\boldsymbol{\tau}^{MN} = \frac{1}{T} \int_0^T \|\boldsymbol{\tau}\| dt$$

where  $T$  is the heartbeat cycle.

## Vorticity

The vorticity vector  $\boldsymbol{\omega}$  can be shown as the outer product of the spatial gradient and the velocity vector.

$$\boldsymbol{\omega} = \nabla \times \mathbf{u}$$

In the two-dimensional case, vectors are always oriented in the z direction, so the direction element can be eliminated and treated as a scalar.

## Cycle

The circulation  $C$  is calculated in terms of the area of the vorticity vector.

$$C = \int_{\Gamma} \boldsymbol{\omega} \cdot \mathbf{n} d\Gamma$$

Although we use the acronym  $C$  for Circulation, many reference books use  $\Gamma$ . Please understand that this book treats  $\Gamma$  as a surface boundary, which is different.

## Helicity

Helicity  $H$  is calculated as follows

$$H = \int_{\Omega} \mathbf{u} \cdot \boldsymbol{\omega} d\Omega$$

The flow is integrated over a region, but  $\mathbf{u}$  and  $\boldsymbol{\omega}$  are sometimes calculated and visualized directly in order to look at local flow.

## Appendix2: Papers

The following is a list of references that may be of interest for blood flow analysis, focusing on papers that are closely related to Cardio Flow Design's technology. Please refer to the website of Cardio Flow Design, Inc. (<https://cfd.life/casereview>), where a series of papers are also introduced.

### Review article

---

Paper	Summary
Itatani K, Yamagishi M, Maeda Y, et al. Adult Congenital Heart Surgery as a Novel Specialty in Thoracic Surgery; Perioperative Patient Management and Surgical Procedures. <i>Kyobu Geka</i> . 2019;72(4):297-305.	New methods for determining surgical indications, processes, and perioperative management using 4D Imaging in adult congenital heart disease are presented.
Itatani K, Miyazaki S, Furusawa T, et al. New imaging tools in cardiovascular medicine: computational fluid dynamics and 4D flow MRI. <i>Gen Thorac Cardiovasc Surg</i> . 2017;65(11):611-621. doi:10.1007/s11748-017-0834-5	This is a comprehensive review of blood flow analysis techniques such as 4D Flow, CFD, and VFM. The basics of typical blood flow imaging modalities and their applications are discussed.
Itatani K, Yamagishi M, Yaku H. Role of Blood Flow Imaging in Treating Congenital Heart Disease in Clinical Practice. <i>Pediatr Cardiol Card Surg</i> . 2017;33(5):371-384. doi:10.9794/jspccs.33.371	This is a comprehensive review of the application of 4D Flow, VFM, and CFD in congenital heart disease. The fundamentals of fluid mechanics, the role of each modality, and how to use them are discussed in detail. It is a bibliography in Japanese.



Paper	Summary
Morichi H, Itatani K, Yamazaki S, et al. Influences of Mitral Annuloplasty on Left Ventricular Flow Dynamics Assessed with 4D flow MRI. <i>J Thorac Cardiovasc Surg.</i> Published online 2020. doi:10.1016/j.jtcvs.2020.04.127	This paper measures the effects of LV energy loss, vortex flow, and aortic blood flow in mitral valve repair from 4D Flow. It is reported that intracardiac vortex flow patterns after mitral valve repair are different from those of healthy patients, and that the balance between valve ring size and patient size leads to worse energy loss.
Takigami M, Itatani K, Nakanishi N, et al. Evaluation using a four-dimensional imaging tool before and after pulmonary valve replacement in a patient with tetralogy of Fallot: A case report. <i>J Med Case Rep.</i> 2019;13(1). doi:10.1186/s13256-018-1964-9	This case report analyzes the hemodynamic changes before and after reoperation for tetralogy of Fallot. The report describes the usefulness of 4D Flow MRI in guiding reoperation by comprehensively evaluating the pathophysiology by measuring energy loss, cardiac coefficient, and other parameters from MRI.
Fujita S, Yamagishi M, Miyazaki T, et al. Hemodynamics Assessment with Four-Dimensional Flow MRI for a Case of Total Cavopulmonary Connection with Extracardiac Conduit Kinking and Protein-Losing Enteropathy. <i>Pediatr Cardiol Card Surg.</i> 2018;34(4):197-204. doi:10.9794/jspccs.34.197	This is a case report on understanding the pathophysiology of a TCPC patient from 4D Flow MRI blood flow analysis. Using the maximum information available from 4D Flow MRI, such as superior and inferior vena cava flow, turbulent blood flow, WSS, energy loss, etc., the relationship with the pathophysiology is carefully interpreted, and this report is helpful in connecting 4D Flow MRI analysis to clinical practice.
Takei Y, Itatani K, Miyazaki S, Shibasaki I, Fukuda H. Four-dimensional flow magnetic resonance imaging analysis before and after thoracic endovascular aortic repair of chronic type B aortic dissection. <i>Interact Cardiovasc Thorac Surg.</i> 2019;28(3):413-420. doi:10.1093/icvts/ivy271	We have measured entry flow and false lumen flow volumes before and after treatment of aortic dissection by 4D Flow MRI and reported the hemodynamic impact of entry closure.
Shibata M, Itatani K, Hayashi T, et al. Flow Energy Loss as a Predictive Parameter for Right Ventricular Deterioration Caused by Pulmonary Regurgitation After Tetralogy of Fallot Repair. <i>Pediatr Cardiol.</i> 2018;39(4):731-742. doi:10.1007/s00246-018-1813-z	This is a paper on blood flow analysis using VFM and 2D Cine PCMRI in tetralogy of Fallot to measure energy loss. It evaluates blood flow in RVOT and shows that VFM with 2D flow limitation is sufficient to evaluate blood flow and that VFM is useful in the evaluation of TOF.
Miyazaki S, Itatani K, Furusawa T, et al. Validation of numerical simulation methods in aortic arch using 4D Flow MRI. <i>Heart Vessels.</i> 2017;32(8):1032-1044. doi:10.1007/s00380-017-0979-2	This is a report of cross-validation between 4D Flow MRI and CFD in aortic blood flow analysis, examining the impact of the lack of spatial resolution in 4D Flow MRI and the choice of model in CFD on WSS and Energy Loss.

Paper	Summary
Miyaji K, Miyazaki S, Itatani K, Oka N, Kitamura T, Horai T. Novel surgical strategy for complicated pulmonary stenosis using haemodynamic analysis based on a virtual operation with numerical flow analysis. <i>Interact Cardiovasc Thorac Surg.</i> 2019;28(5):775-782. doi:10.1093/icvts/ivy326	This is a report on the optimization of surgical procedures for pulmonary artery stenosis using virtual surgical simulation; in addition to CFD, a 3D modeling technique is used to create a blueprint of the patches.
Asada S, Yamagishi M, Itatani K, et al. Early outcomes and computational fluid dynamic analyses of chimney reconstruction in the Norwood procedure. <i>Interact Cardiovasc Thorac Surg.</i> 2019;29(2):252-259. doi:10.1093/icvts/ivz040	This is a report on CFD analysis of blood flow in the aorta reconstructed by the Chimney method in HLHS, verifying that the method is efficient with less hemodynamic turbulence.
Miyazaki S, Miyaji K, Itatani K, et al. Surgical strategy for aortic arch reconstruction after the Norwood procedure based on numerical flow analysis. <i>Interact Cardiovasc Thorac Surg.</i> 2018;26(3):460-467. doi:10.1093/icvts/ivx332	This paper examines the relationship between the geometrical and hemodynamic characteristics of the reconstructed aorta after the Norwood procedure.
Kato N, Yamagishi M, Itatani K, et al. Effects of blood flow dynamics on autologous pericardial degeneration in reconstructed pulmonary arteries. <i>Interact Cardiovasc Thorac Surg.</i> 2018;26(2):293-300. doi:10.1093/icvts/ivx293	This is a paper that measures WSS, OSI by CFD in pulmonary arteries reconstructed with autologous pericardium and aortopulmonary collateral arteries.
Numata S, Itatani K, Kawajiri H, Yamazaki S, Kanda K, Yaku H. Computational fluid dynamics simulation of the right subclavian artery cannulation. <i>J Thorac Cardiovasc Surg.</i> 2017;154(2):480-487. doi:10.1016/j.jtcvs.2017.02.073	This report examines the changes in aortic blood flow that vary with the insertion position of the sending vessel. The simulation calculates the difference in blood delivery methods in the ascending aorta and right subclavian artery.

Paper	Summary
Kainuma A, Akiyama K, Naito Y, et al. Energetic performance index improvement after Glenn and Damus-Kaye-Stansel procedure using vector flow mapping analysis: a case report. <i>JA Clin Reports</i> . 2020;6(1). doi:10.1186/s40981-020-0312-4	This paper analyzes the energy loss of Glenn surgery and DKS anastomosis using VFM. It reports that the surgery reduces cardiac load.
Hayashi H, Akiyama K, Itatani K, et al. A novel in vivo assessment of fluid dynamics on aortic valve leaflet using epi-aortic echocardiogram. <i>Echocardiography</i> . 2020;37(2):323-330. doi:10.1111/echo.14596	This is a report on the measurement of WSS and OSI of the aortic valve by VFM, which is difficult to measure by CFD and MRI, showing the usefulness of VFM.
Akiyama K, Ji R, Stöhr EJ, et al. Assessment of Wall Shear Stress on the Aortic Valve in Patients with Left Ventricular Assist Device Using Vector Flow Mapping. <i>J Hear Lung Transplant</i> . 2019;38(4):S452. doi:10.1016/j.healun.2019.01.1152	This is a report of VFM analysis of the left ventricle after LVAD transplantation. WSS and OSI of the left ventricle and valve leaflets were measured after transplantation, and the possibility that Denovo's aortic regurgitation is related to low WSS is reported.
Akiyama K, Colombo PC, Stöhr EJ, et al. Blood Flow Kinetic Energy of Right Ventricular Outflow Tract: A Marker for Right Ventricular Global Systolic Function. <i>J Hear Lung Transplant</i> . 2019;38(4):S449-S450. doi:10.1016/j.healun.2019.01.1146	This is a case study of RV dysfunction after LVAD implantation as measured by VFM. RV performance is measured by energy loss.
Kinoshita M, Akiyama K, Itatani K, et al. Energetic performance analysis of staged palliative surgery in tricuspid atresia using vector flow mapping. <i>Cardiovasc Ultrasound</i> . 2017;15(1). doi:10.1186/s12947-017-0118-3	This is a report on the intraoperative energy loss and kinetic energy of BT shunts measured using VFM.
Honda T, Itatani K, Takashi M, et al. Exploring energy loss by vector flow mapping in children with ventricular septal defect: Pathophysiologic significance. <i>Int J Cardiol</i> . 2017;244:143-150. doi:10.1016/j.ijcard.2017.06.035	This is an analysis of children with VFM; the characteristics of intraventricular energy loss in VSD are reported.
Akiyama K, Naito Y, Kinoshita M, et al. Flow Energy Loss Evaluation in a Systolic Anterior Motion Case After the Ross Procedure. <i>J Cardiothorac Vasc Anesth</i> . 2017;31(6):2118-2122. doi:10.1053/j.jvca.2017.03.006	This report analyzes blood flow after Ross surgery with VFM. It describes the mechanism by which ejection fraction and vortex flow cause systolic anterior motion and how it increases energy loss.
Nakashima K, Itatani K, Kitamura T, et al. Energy dynamics of the intraventricular vortex after mitral valve surgery. <i>Heart Vessels</i> . 2017;32(9):1123-1129. doi:10.1007/s00380-017-0967-6	Blood flow after mitral valve surgery has been analyzed by VFM, and it has been reported that the direction of vortical flow changes depending on the surgical technique, affecting energy loss.
Akiyama K, Nakamura N, Itatani K, et al. Flow-dynamics assessment of mitral-valve surgery by intraoperative vector flow mapping. <i>Interact Cardiovasc Thorac Surg</i> . 2017;24(6):869-875. doi:10.1093/icvts/ivx033	Blood flow after mitral valve surgery has been analyzed by VFM and the relationship between valve angle and vortex pattern and energy loss has been reported.

Paper	Summary
<p>Shigemitsu S, Takahashi K, Yazaki K, et al. New insight into the intraventricular pressure gradient as a sensitive indicator of diastolic cardiac dysfunction in patients with childhood cancer after anthracycline therapy. <i>Heart Vessels</i>. 2019;34(6):992-1001. doi:10.1007/s00380-018-01332-7</p>	<p>A report on hemodynamic analysis of the effects of anthracycline chemotherapy on cardiotoxicity states that left ventricular IVPG is useful in assessing early cardiotoxicity. The report describes the usefulness of IVPG in comparison with the currently prevailing short-axis and long-axis Strain analysis.</p>
<p>Takahashi K, Nii M, Takigiku K, et al. Development of suction force during early diastole from the left atrium to the left ventricle in infants, children, and adolescents. <i>Heart Vessels</i>. 2019;34(2):296-306. doi:10.1007/s00380-018-1239-9</p>	<p>This paper determines age-specific IVPG norms in children with normal IVPG.</p>
<p>Yamamoto Y, Takahashi K, Takemoto Y, et al. Evaluation of Myocardial Function According to Early Diastolic Intraventricular Pressure Difference in Fetuses. <i>J Am Soc Echocardiogr</i>. 2017;30(11):1130-1137.e1. doi:10.1016/j.echo.2017.07.013</p>	<p>This is a report on the measurement of IVPG in fetuses. The characteristics of IVPG in the fetus are described, including its relationship to the duration of gestation, heart size, and cardiac output.</p>
<p>Kobayashi M, Takahashi K, Yamada M, et al. Assessment of early diastolic intraventricular pressure gradient in the left ventricle among patients with repaired tetralogy of Fallot. <i>Heart Vessels</i>. 2017;32(11):1364-1374. doi:10.1007/s00380-017-1011-6</p>	<p>This is a paper from IVPG on the mechanisms of postoperative diastolic function after Fallot surgery.</p>

# References

1. Roguin A, Scipione Riva-Rocci and the men behind the mercury sphygmomanometer. *Int J Clin Pract.* 2005;60(1):73-79. doi:10.1111/j.1742-1241.2005.00548.x
2. Töger J, Kanski M, Carlsson M, et al. Vortex Ring Formation in the Left Ventricle of the Heart: Analysis by 4D Flow MRI and Lagrangian Coherent Structures. *Ann Biomed Eng.* 2012;40(12):2652-2662. doi:10.1007/s10439-012-0615-3
3. Frydrychowicz A, Berger A, Munoz Del Rio A, et al. Interdependencies of aortic arch secondary flow patterns, geometry, and age analysed by 4-dimensional phase contrast magnetic resonance imaging at 3 Tesla. *Eur Radiol.* 2012;22(5):1122-1130. doi:10.1007/s00330-011-2353-6
4. Katayama S, Umetani N, Sugiura S, Hisada T. The sinus of Valsalva relieves abnormal stress on aortic valve leaflets by facilitating smooth closure. *J Thorac Cardiovasc Surg.* 2008;136(6):1528-1535. doi:10.1016/j.jtcvs.2008.05.054
5. Kakizaki R, Honda T, Miyazaki S, Itatani K. 右心機能を考えるうえで知っておくべき基本とは? *Hear View.* 2015;19(3):260-267.
6. Pinsky MR. Determinants of pulmonary arterial flow variation during respiration. *J Appl Physiol Respir Environ Exerc Physiol.* 1984;56(5):1237-1245. doi:10.1152/jappl.1984.56.5.1237
7. Tsubata H, Nakanishi N, Itatani K, Ogo T, Yaku H, Matoba S. Pulmonary artery blood flow dynamics in patients with chronic thromboembolic pulmonary hypertension; Analysis by computational fluid dynamics. In: *European Respiratory Society (ERS); 2019:PA1435.* doi:10.1183/13993003.congress-2019.pa1435
8. Kameneva M V, Burgreen GW, Kono K, Repko B, Antaki JF, Umezumi M. Effects of turbulent stresses upon mechanical hemolysis: Experimental and computational analysis. *ASAIO J.* 2004;50(5):418-423. doi:10.1097/01.MAT.0000136512.36370.B5
9. Nakahara T, Yoshida F. Mechanical effects on rates of hemolysis. *J Biomed Mater Res.* 1986;20(3):363-374. doi:10.1002/jbm.820200308
10. Davies PF, Remuzzi A, Gordon EJ, Dewey CF, Gimbrone MA. Turbulent fluid shear stress induces vascular endothelial cell turnover in vitro. *Proc Natl Acad Sci U S A.* 1986;83(7):2114-2117. doi:10.1073/pnas.83.7.2114
11. Ito Y, Nakamura S, Sugimoto N, et al. Turbulence Activates Platelet Biogenesis to Enable Clinical Scale Ex Vivo Production. *Cell.* 2018;174(3):636-648.e18. doi:10.1016/j.cell.2018.06.011
12. 立石実, 板谷慶一, 宮崎翔平, et al. 右室流出路再建後遠隔期狭窄における狭窄形態と血流動態からみた重症度評価と治療戦略. Presented at the: 2013.
13. Miyazaki S, Miyaji K, Itatani K, et al. Surgical strategy for aortic arch reconstruction after the Norwood procedure based on numerical flow analysis. *Interact Cardiovasc Thorac Surg.* 2018;26(3):460-467. doi:10.1093/icvts/ivx332
14. Geiger J, Arnold R, Herzer L, et al. Aortic wall shear stress in Marfan syndrome. *Magn Reson Med.* 2013;70(4):1137-1144. doi:10.1002/mrm.24562
15. Hope T a, Herfkens RJ. Imaging of the thoracic aorta with time-resolved three-dimensional phase-contrast MRI: a review. *Semin Thorac Cardiovasc Surg.* 2008;20(4):358-364. doi:10.1053/j.semtcvs.2008.11.013
16. 1Markl M, Frydrychowicz A, Kozerke S, Hope M, Wieben O. 4D flow MRI. *J Magn Reson Imaging.* 2012;36(5):1015-1036. doi:10.1002/jmri.23632
17. 住谷拓斗, 板谷慶一, 中村匡徳. 仮想ドブラデータによる3次元的VFMの実現に向けた計算方法の検討. In: 第11回血流通会.; 2019.
18. 板谷慶一. 医学・医療のためのコンピューターシミュレーション技術の開発現場の臨床現場の実情とあり方. 第2回コンピューターシミュレーション専門部会、独立行政法人医薬品医療機器総合機構. Published 2020. Accessed August 28, 2020. <https://www.pmda.go.jp/rs-std-jp/subcommittees/0004.html>
19. akigami M, Itatani K, Nakanishi N, et al. Evaluation using a four-dimensional imaging tool before and after pulmonary valve replacement in a patient with tetralogy of Fallot: A case report. *J Med Case Rep.* 2019;13(1). doi:10.1186/s13256-018-1964-9
20. akei Y, Itatani K, Miyazaki S, Shibasaki I, Fukuda H. Four-dimensional flow magnetic resonance imaging analysis before and after thoracic endovascular aortic repair of chronic type B aortic dissection. *Interact Cardiovasc Thorac Surg.* 2019;28(3):413-420. doi:10.1093/icvts/ivy271
21. Miyaji K, Miyazaki S, Itatani K, Oka N, Kitamura T, Horai T. Novel surgical strategy for complicated pulmonary stenosis using haemodynamic analysis based on a virtual operation with numerical flow analysis. *Interact Cardiovasc Thorac Surg.* 2019;28(5):775-782. doi:10.1093/icvts/ivy326
22. Miyazaki S, Miyaji K, Itatani K, et al. Surgical strategy for aortic arch reconstruction after the Norwood procedure based on numerical flow analysis. *Interact Cardiovasc Thorac Surg.* 2018;26(3):460-467. doi:10.1093/icvts/ivx332
23. Nakashima K, Itatani K, Kitamura T, et al. Energy dynamics of the intraventricular vortex after mitral valve surgery. *Heart Vessels.* 2017;32(9):1123-1129. doi:10.1007/s00380-017-0967-6
24. Itatani K, Ono M. 血流可視化診断装置、及びプログラム. Published online 2011.
25. Chatzizisis YS, Coskun AU, Jonas M, Edelman ER, Feldman CL, Stone PH. Role of endothelial shear stress in the natural history of coronary atherosclerosis and vascular remodeling: molecular, cellular, and vascular behavior. *J Am Coll Cardiol.* 2007;49(25):2379-2393. doi:10.1016/j.jacc.2007.02.059
26. Les AS, Shadden SC, Figueroa CA, et al. Quantification of hemodynamics in abdominal aortic aneurysms during rest and exercise using magnetic resonance imaging and computational fluid dynamics. *Ann Biomed Eng.* 2010;38(4):1288-1313. doi:10.1007/s10439-010-9949-x



My perfect match with Fluid Mechanics and Cardiac Surgery.

When I was a medical student, I used to be an edgy personality. It was not unusual at that time for medical students to pass entrance exams with highly deviated scores in mathematics and physics, so the dominant public opinions often tended to be too biased on humanity rather than scientific talents for clinicians against fierce competitive Japanese medical school entrance exams. However, in these era, I felt such opinion leaders in media or education shady, and even thought that "I would lose out, if I serve society". I read a large number of textbooks in mathematics and physics, and finally was amused by the conflict between physics, which uses theory to explain phenomena, and mathematics, which pursues a completely consistent theory. In medical school, students were crammed with a huge amount of knowledge on genes and diseases, and on clinical guidelines, and I had a hard time understanding why the stance on science in medicine was so different from that of quantum field theory, which aims for the grand unified theory.

The turning point for me came when I encountered a child with univentricular heart who underwent Fontan procedure in the practical training for medical students. The child, who was still very young, had undergone numerous surgeries and finally reached to a mysterious hemodynamic state. I was strongly motivated to scientifically design the procedure based on accurate calculation because in an era when even car engines were meticulously blueprinted, the heart, the power source of human life, should never be neither calculated nor designed. I was confident that the problem could not be solved by leaving it to genes and statistics, and I decided to start a career as a cardiac surgeon but with fluid dynamics, the physics of nonlinear non-conservative systems for complex phenomena.

Ten years later, the results of numerical calculations of the optimal graft size and pulmonary arterial size for the Fontan procedure attracted attention at an international conference of thoracic surgery. However, some physicians criticized them for not being actual measurements. Therefore, I developed blood flow visualization devices based on echocardiography and cardiac MRI. Rather than beautiful movies that nobody has seen before, my interest was focused on "what is the ideal blood flow for human life system" and I also thought that a study that could not save lives had no value.

Later, I met a lot of patients after the repair of congenital heart diseases. These were patients whom I had to encounter, for whom there were certainly no treatment guidelines, no reports of experiences, and the only solution was the blood flow analysis that I had developed. I felt as if I had seen the existence of the only solution to one of the unsolved problems of mathematics in this century, fluid dynamics, in their surgical techniques, and I put it into practice. There was a medicine and a science that lived together with the patients. Clinical medicine is a science with quite broad background, and I believe that blood flow analysis is one of its frames of reference.

Keiichi Itatani MD, PhD.

The story of how I met the two key persons and how it all began.

According to my Google calendar, the first time I met Keiichi Itatani was on April 8, 2015, at 3 pm. I still clearly remember that scene even now. One of the physicians who worked at my medical corporation, Yukoukai, agreed to meet with me because he had an interesting person, he wanted to match me up with.

The name of the person is Keiichi Itatani. He is a doctor.

He was one year younger than me, and during his six years at the University of Tokyo School of Medicine, he had been fascinated with mathematics and physics, especially fluid dynamics, which he had taught himself. He also said that since becoming a cardiac surgeon, he has programmed his own software to analyze blood flow using fluid dynamics. His hobby is playing the piano, and he is a professional-level player. Even before meeting him, I was already looking forward to seeing what kind of a crazy guy he would be.

On the day of the meeting, Dr. Itatani was accompanied by a young man named Shohei Miyazaki (currently CTO of CardioFlowDesign), who had just graduated from Waseda University and had worked with Dr. Itatani as a research assistant at Kitasato University.

I asked Dr. Itatani what he was researching. From that moment on, the endless machine gun talk began. He explained everything from his research since he was a student from the development of software, its medical usefulness, and its social significance, all rationally and without a single cloud of doubt. It was a story of medical research so grand that I would have never thought about, and I was in a situation where I could not catch up with my understanding, so I asked a lot of questions in an attempt to resolve the parts I did not understand. I asked every question I could think of, and he answered every question perfectly, without the slightest hesitation. He had already said from that time that cardiac surgery was to quantitatively evaluate the fluid inside the heart with the concept of blood flow analysis and correct it to the correct blood flow during surgery.

I thought, "This is truly a project to eliminate the hand of God from the field of cardiac surgery." I have seen many prodigies in universities and hospitals, but he is a genius of a different caliber.

My brain was already at 30% more blood flow at that moment, and I couldn't think straight. But I knew that the work he had done so far alone should be commercialized immediately and delivered to many people. I felt certain that if we did not make the new medicine of blood flow analysis known and used by cardiac surgeons, cardiologists, and radiologists around the world soon, many lives that could be saved now would be lost.

About 30 minutes into our conversation, I enthusiastically invited Dr. Itatani to form a company and make this a business. I remember that I told him that I would be willing to invest all of my funds. But I was unaware of the enormous research and development costs that would be required to turn it into a medical device. And later I would become frightened at the scale of the costs.

Before that, there were several problems with the commercialization of the project.

When I asked him about the situation, he told us that Dr. Itatani, who was then an associate professor of Kitasato University's endowed chair, had decided to close the chair and move to another research institute by himself due to differences in policy with the chief professor of Kitasato University and the donor of the endowed chair. And Shohei Miyazaki is also going to work for a certain major company. This meant that all the staff members, including those at Kitasato University, were now scattered, and it was no longer possible for them to work together on software development.

I felt that at least Dr. Miyazaki should join the project, so I called him later and told him, "If you don't trust me and participate in this project, we won't do it either."

Actually, I thought I would do it even if he didn't come.

A few weeks later, Dr. Miyazaki contacted me and said he wanted to join us in the project.

On August 18, 2015, CardioFlowDesign Inc. was founded. And that day was the birthday of Brooke Taylor, who discovered the "Taylor Expansion"

That day marked the beginning of our challenge to bring the concept of quantitative evaluation to the field of cardiac surgery and cardiology through blood flow analysis.

Now, after 7 years in business, we have many of the domestic facilities that perform cardiac surgery as clients and are preparing to bring blood flow analysis to the entire world next.

## An Encouragement of Blood Flow Analysis

---

Published 3rd edition November 27, 2022

---

Supervised by Keiichi Itatani

Produced by Cardio Flow Design Inc.

22-3, Ichibancho, Chiyoda, Tokyo

---